Knocking out non-muscle myosin II in retinal ganglion cells promotes long-distance optic nerve regeneration

Xue-Wei Wang[1, #], Shu-Guang Yang[1, #], Chi Zhang[1, #], Jin-Jin Ma[3], Yingchi Zhang[1], Bin-Bin Yang[1], Yi-Lan Weng[5], Guo-Li Ming[6], Anish R. Kosanam[1], Saijilafu [3,4, *], and Feng-Quan Zhou[1, 2, *]

[1]Department of Orthopaedic Surgery, The Johns Hopkins University School of Medicine, Baltimore, MD 21287

[2]The Solomon H. Snyder Department of Neuroscience, The Johns Hopkins University School of Medicine, Baltimore, MD 21287

[3]Orthopaedic Institute, Medical College, Soochow University, Suzhou, Jiangsu, China

[4]Department of Orthopaedic Surgery, the First Affiliated Hospital, Soochow University, Suzhou, China

[5]Center for Neuroregeneration, Department of Neurosurgery, Houston Methodist Research Institute, Houston, TX 77030

[6]Department of Neuroscience, Perelman School of Medicine, University of Pennsylvania, Philadelphia, PA 19104

[#]These authors contributed equally to this study

*Correspondence to:

Feng-Quan Zhou, Ph.D., Room 291, The John G. Rangos Sr. Building, 855 North Wolfe Street, Baltimore, MD 21287, Email: fzhou4@jhmi.edu

Saijilafu, Ph.D. Orthopaedic Institute, Medical College, Soochow University, Suzhou, Jiangsu, China

Email: saijilafu@suda.edu.cn

Summary

In addition to changed gene expression, pathological cytoskeletal dynamics in the axon is another key intrinsic barrier for axon regeneration in the central nervous system (CNS). Here we showed that knocking out myosin IIA/B in retinal ganglion cells alone was sufficient to induce marked and sustained optic nerve regeneration. Combined Lin28 overexpression and myosin IIA/B knockout led to remarkable synergistic promoting effect and long-distance axon regeneration. Immunostaining, RNA-seq and western blot analyses revealed that myosin II deletion did not affect known axon regeneration signaling pathways or the expression of regeneration associated genes. Instead, it abolished the retraction bulb formation and significantly enhanced the axon extension efficiency. The study provided clear and strong evidence that directly targeting neuronal cytoskeleton was sufficient to induce strong CNS axon regeneration, and combining gene expression in the soma and modified cytoskeletal dynamics in the axon was an optimal approach for long-distance CNS axon regeneration.

Keywords

Axon regeneration, optic nerve regeneration, non-muscle myosin II, Lin28, growth cone, cytoskeleton

Introduction

Axon regeneration in the mammalian central nervous system (CNS) has been a long standing and highly challenging issue in the biomedical research field. The current consensus is that there are two major reasons that neurons in the mature mammalian CNS do not regenerate their axons after the injury. One is the hostile environment caused by inhibitors in the scar tissues and degenerating myelin, and the other is the diminished intrinsic neural regeneration ability of mature CNS neurons[1,2]. Therefore, the widely accepted view is that combination strategies that target both intrinsic growth ability and inhibitory environment are likely the best option for successful CNS axon regeneration and function recovery. Early studies[3-6] using peripheral nerve graft transplants have shown that some mature CNS neurons, such as spinal cord neurons and retinal ganglion cells (RGCs), could regenerate their axons into the permissive nerve grafts, indicating clearly that these neurons still retain limited intrinsic regeneration ability. However, to date many studies targeting selected inhibitory molecules resulted in no or very modest CNS regeneration[7,8]. A likely reason is that there are multiple classes of inhibitory molecules, potentially including unidentified ones, which inhibit axon regeneration via distinct cellular and molecular mechanisms. Thus, targeting a few inhibitory signals while leaving the others intact may not result in a permissive environment similar to that in the peripheral nerve grafts.

In contrast, several studies targeting the intrinsic axon growth ability (e.g. Pten, SOCS3, KLF4, Lin28)[9-13] have produced very promising results. However, in the corticospinal tract (CST) regeneration model, although modulation of the intrinsic regeneration ability substantially enhanced axon regeneration, most regenerating axons still cannot pass the lesion site, likely due to the effects of inhibitory molecules at the injury site, especially glial scar-based inhibitors. For instance, Pten deletion has been shown to induce by far the strongest promoting effect on CST axon regeneration[9]. However, the most robust promoting effect can only be achieved in young mice (< 1 month). A recent study[14] showed that Pten

67 deletion-induced regeneration of CST axons beyond the injury site was greatly diminished in aged mice.
68 Specifically, in 12-18-month-old mice, Pten deletion led to little, if any, CST regeneration beyond the
69 injury site. One likely reason for the diminished effect in older animals was the increased response to the
70 inhibitory CNS environment. Thus, developing a successful strategy for stimulating regeneration of
71 injured CST remains a challenge, especially in older animals. In the optic nerve regeneration model,
72 boosting the intrinsic regeneration ability of RGCs have produced strong optic nerve regeneration.
73 However, tissue clearing and 3D imaging studies have revealed that many of the regenerating RGC axons
74 make U-turns in the optic nerve, at the optic chiasm, or make wrong guidance decisions after the
75 chiasm[15,16]. Together, a new strategy is needed to enable neurons with increased intrinsic axon growth
76 ability to grow axons in the inhibitory environment more efficiently with less U-turns and unnecessary
77 branching, and can cross the inhibitory boundary more efficiently.

78 Neuronal cytoskeleton is not only the major machinery that drives axon growth[17-19], but also the
79 converging targets of most, if not all, inhibitory signaling pathways[17,19]. In other words, by directly
80 manipulating growth cone cytoskeletal motility it is possible to interfere with how the growth cones
81 respond to multiple inhibitory signals, regardless if these signals are from different inhibitors or
82 downstream pathways. Indeed, our previous study[20] showed that knocking down or pharmacologically
83 inhibiting non-muscle myosin IIA/B could allow regenerating sensory axons to grow straight, make less
84 branches, and completely ignore chondroitin sulfate proteoglycans (CSPGs) and myelin-based inhibitors.
85 The effects were much stronger than that of Rho kinase inhibitor. Here we examined if knocking out non-
86 muscle myosin IIA/B in RGCs could promote optic nerve regeneration in vivo. The results showed that
87 deleting myosin IIA/B alone was sufficient to induce robust and sustained optic nerve regeneration.
88 Moreover, combination of myosin IIA/B knockout and Lin28 overexpression, which enhances the
89 intrinsic axon regeneration ability of RGCs[13], led to synergistic promoting effect and surprisingly long-

90 distance optic nerve regeneration. Importantly, the promoting effect was independent of well-known
91 signaling mediators of optic nerve regeneration, such as increased mTOR activity and GSK3β
92 inactivation[2]. RNA-seq and western blot analyses comparing wild type and myosin IIA/B knockout
93 neurons showed no significant difference in the expression of known regeneration associated genes,
94 indicating local effects in the axons. In support, detailed analyses of growth cone morphologies and axon
95 trajectories revealed that myosin II deletion almost abolished the formation of retraction bulbs, a hallmark
96 of failed axon regeneration, and significantly enhanced the axon extension efficiency in the optic nerve.
97 Collectively, our study demonstrated clearly that manipulation of neuronal cytoskeleton alone was
98 sufficient to promote significant CNS axon regeneration in vivo. The study also provided strong evidence
99 that combining enhanced intrinsic regeneration ability in the neuronal soma with local manipulation of
100 axonal cytoskeleton was an optimal approach to induce long-distance CNS axon regeneration in vivo.
101

102 **Results**

103 **Double knockout of non-muscle myosin IIA/B in RGCs led to significant and sustained optic nerve**
104 **regeneration in vivo**

105 Non-muscle myosin II consists of two essential light chains, two regulatory light chains, and a
106 myosin II heavy chain (MHC). There are three different isoforms of MHCs in mammalian cells, IIA, IIB,
107 and IIC, encoded by *Myh 9*,*10*, and *14* genes, respectively. Myosin IIA and IIB with MHC IIA/B (myosin
108 IIA/B) are the major isoforms in neurons[20]. In nerve growth cones, both myosin IIA/B are localized near
109 the transition zone, where microtubules and actin filaments interact[20]. Our previous study[20] has shown that
110 pharmacological inhibition or double knockdown of myosin IIA/B in developing or regenerating sensory
111 neurons drastically promoted sensory axon growth over two major inhibitory substrates, myelin extracts
112 or CSPGs. Here we tested if myosin IIA/B loss of function could also induce axon regeneration in RGCs
113 after optic nerve injury. To knock out both myosin IIA/B in RGCs, we crossed *Myh9*$^{f/f}$ and *Myh10*$^{f/f}$ mice
114 to generate *Myh9*$^{f/f}$*: Myh10*$^{f/f}$ mice (hereafter *myosin IIA/B*$^{f/f}$), and injected AAV2-Cre into the vitreous
115 humors of these mice. Wild type mice injected with AAV2-Cre were used in the control group. To
116 examine viral vector infection rate, immunostaining of Cre recombinase in whole-mount retina was
117 performed two weeks after the injection. The results showed that the infection rate in RGCs was about
118 90% (Supplementary Figure 1A, C). Immunostaining of retinal sections also showed a nice colocalization
119 of Cre staining with Tuj1-positive RGCs (Supplementary Figure 1B). We also injected AAV2-Cre into
120 tdTomato reporter mice to examine the efficiency of Cre-mediated gene recombination. Strong expression
121 of tdTomato in RGCs was observed two weeks after AAV2-Cre injection (Supplementary Figure 2A, B),
122 indicating successful gene recombination. Lastly, we examined if myosin IIA/B were indeed deleted in
123 RGCs after AAV2-Cre injection. By western blot analysis of the whole retina tissue, we found that the
124 protein level of myosin IIA was markedly reduced (Supplementary Figure 3A). Immunostaining of retinal

125 sections with anti-myosin IIB antibody showed significantly reduced level of myosin IIB in RGCs
126 (Supplementary Figure 3B, C). Together, these results demonstrated clearly that myosin IIA/B were
127 successfully deleted in RGCs.

128 To determine how myosin IIA/B double knockout (dKO) in RGCs affected optic nerve
129 regeneration, we performed optic nerve crush (ONC) 2 weeks after the viral injection. We first assessed
130 optic nerve regeneration 2 weeks after the ONC. The regenerating RGC axons were labeled with
131 anterogradely transported cholera toxin subunit B (CTB) conjugated with Alexa Fluor 594, which was
132 injected into the vitreous humor 2 days prior to tissue harvest (Figure 1A). The fixed optic nerves were
133 first tissue cleared to be transparent as previously described[13] and axon regeneration was imaged with
134 confocal microscopy. The results showed that very limited optic nerve regeneration occurred in wild type
135 mice infected with AAV2-Cre. In contrast, there was greatly enhanced optic nerve regeneration in myosin
136 IIA/B dKO mice (Figure 1A, B). In the majority of optic nerves, regenerating axons reached 750 μm from
137 the crush site. To further determine if myosin IIA/B dKO led to sustained promoting effect on optic nerve
138 regeneration, we assessed optic nerve regeneration 4 weeks after the ONC. We found that at 4 weeks post
139 ONC myosin IIA/B dKO significantly increased not only the lengths but also the number of regenerating
140 axons, indicating continued axon regeneration along time. Specifically, most optic nerves had regenerating
141 axons reaching 2000 μm from the crush site (Figure 1B). In addition to counting axon numbers at different
142 distances from the crush site, we also quantified the lengths of the top 5 longest regenerating axons in
143 each condition. The result showed that in control condition the lengths of the top 5 axons remained
144 unchanged at 2 and 4 weeks, whereas the top 5 axons of myosin IIA/B dKO RGCs continued to grow
145 from 2 to 4 weeks (Figure 1C). Both quantification results demonstrated that knocking out myosin IIA/B
146 in RGCs led to sustained optic nerve regeneration at the same speed up to 4 weeks. When RGC survival
147 rates were assessed, myosin IIA/B dKO showed no effect (Figure 1D, E), indicating that it promoted optic

148 nerve regeneration by enhancing axon extension rather than protecting RGCs from ONC-induced cell
149 death. Collectively, these results demonstrated clearly that knocking out myosin IIA/B was sufficient to
150 induce robust and sustained optic nerve regeneration without affecting cell survival.
151

152 **Knocking out non-muscle myosin IIA/B acted synergistically with Lin28a overexpression to**
153 **promote long-distance optic nerve regeneration**

154 Our recent study showed that overexpression of Lin28 in RGCs induced robust and sustained optic
155 nerve regeneration via regulation of gene expression and enhanced intrinsic axon regeneration ability[13].
156 Therefore, we tested if combining myosin IIA/B dKO, which alters axonal cytoskeletal dynamics, with
157 Lin28 overexpression, which controls gene expression, could have combinatory promoting effect on optic
158 nerve regeneration. The results showed that either myosin IIA/B dKO or Lin28a overexpression alone
159 could lead to robust optic nerve regeneration 2 weeks after ONC (Figure 2A, B). When both treatments
160 were combined, optic nerve regeneration was greatly enhanced, with the longest length reaching 3.5mm
161 from the crush site (Figure 2A, B). In particular, either myosin IIA/B dKO or Lin28a overexpression
162 RGCs had almost no regenerating axons growing beyond 1.75 mm from the crush site. In contrast, in the
163 combinatory treatment group there were significant number of regenerating axons at 3 mm and the longest
164 axons reached up to 3.5 mm (Figure 2A, B). Because the dehydration process in the tissue clearing
165 approach results in 18% of shrinkage in nerve lengths[13], the real lengths of the longest regenerating axons
166 were more than 4 mm. Indeed, in about half of nerves in the combinatory group the longest regenerating
167 axons almost reached the optic chiasm (Figure 2A and Supplementary Figure 4) 2 weeks after ONC. This
168 result suggested that myosin IIA/B dKO and Lin28a acted synergistically to promote long-distance optic
169 nerve regeneration. Similarly, we quantified the average distances of the top 5 longest regenerating axons
170 in each condition. The results showed that the longest regenerating axons in the combinatory group were

171 markedly longer than either the myosin IIA/B dKO or Lin28a overexpression group (Figure 2C). To better
172 show the regenerating axons in the tissue cleared transparent optic nerves, we created a 3D animation of
173 an optic nerve (Supplementary Video 1).
174

175 **Knocking out non-muscle myosin IIA/B in RGCs did not significantly affect known optic nerve**
176 **regeneration signaling pathways**

177 In our previous study[20], we showed that treating adult sensory neurons cultured on CSPGs with
178 the myosin II inhibitor, blebbistatin, could induce halted axon to regrow within minutes. Conversely,
179 washing out the blebbistatin stopped axon growth in a very short time. Such rapid response to blebbistatin
180 in both ways indicated that inhibition of myosin II promoted axon growth by its direct effects on growth
181 cone cytoskeleton without affecting signaling events in the neuronal soma. To test this idea, we examined
182 how myosin IIA/B dKO affected two well-known pathways governing the intrinsic axon regeneration
183 ability, the activation of mTOR, marked by increased level of phospho-S6 (pS6), and the inactivation of
184 GSK3β, marked by phosphorylation of its serine 9 residue (pGSK3β), at 2 weeks after ONC. Previous
185 studies have shown that most identified molecules promoting optic nerve regeneration act via either of
186 these pathways, including Pten knockout[10], Akt overexpression[21,22], Lin28 overexpression[13], osteopontin
187 overexpression[23], SOCS3 deletion[12], melanopsin overexpression[24], HDAC5 manipulation[25], and direct
188 modulation of mTOR[26] or GSK3β signaling[21]. For mTOR activation, we examined the level of pS6 in
189 RGCs under different conditions. The results showed that knocking out myosin IIA/B had no effect on
190 pS6 level, whereas Lin28a overexpression markedly increased the level of pS6 in RGCs (Figure 3A).
191 Quantification demonstrated that the percentage of pS6 positive ($pS6^+$) RGCs increased by nearly 8 folds
192 in the Lin28a overexpression group compared to that in the wild type group, whereas myosin IIA/B dKO
193 had no effect (Fig. 3B). To provide a more objective measurement of pS6 level in RGCs, we also

194 quantified the average fluorescence intensity of pS6 staining in all Tuj1 positive RGCs. The results showed
195 that myosin IIA/B dKO actually slightly but significantly reduced the pS6 level compared to that of the
196 wild type group. In contrast, Lin28a overexpression greatly increased the pS6 level (Figure 3C). Lastly,
197 we quantified the average fluorescence intensity of pS6 staining only in $pS6^+$ RGCs under different
198 conditions. Similarly, there was no significant difference between wild type and myosin IIA/B dKO RGCs,
199 whereas the Lin28a overexpression group had a much higher value (Figure 3D).

200 For GSK3β inactivation, we found that there was very few wild type RGCs showing positive
201 staining of pGSK3β, and knocking out myosin IIA/B had no impact on it (Figure 3E, F). In contrast,
202 Lin28a overexpression increased the percentage of pGSK3β positive ($pGSK3\beta^+$) RGCs by about 6 folds
203 (Figure 3F). The average fluorescence intensity of pGSK3β staining in all Tuj1 positive RGCs was not
204 affected by myosin IIA/B dKO, whereas Lin28a overexpression greatly increased the pGSK3β level
205 (Figure 3G). When the average fluorescence intensity of pGSK3β were quantified only in $pGSK3\beta^+$ RGCs,
206 the level of pGSK3β was significantly decreased in myosin IIA/B dKO group compared with that in the
207 wild type group. The level of pGSK3β in the Lin28a overexpression group was still the highest (Figure
208 3H).

209 Taken together, these results provided clear and strong evidence that knocking out myosin IIA/B
210 had no effects on two well-known signaling pathways occurred in the neuronal soma supporting intrinsic
211 regenerative ability of optic nerves.

212

213 **Knocking out non-muscle myosin IIA/B in sensory neurons did not significantly affect known**
214 **regeneration associated genes and pathways**

215 To further explore the potential molecular mechanisms underlying myosin IIA/B dKO induced
216 axon regeneration, we performed sham surgery or bilateral sciatic nerve injury (SNI) on *myosin IIA/B*$^{f/f}$

217 and *Advillin-Cre: myosin IIA/B*$^{f/f}$ mice, in which myosin IIA/B were conditionally knocked out in sensory
218 neurons. Three days later, we collected lumbar 4 and 5 dorsal root ganglia (L4/5 DRGs) and isolated
219 mRNA and protein for RNA-seq and western blot analyses. As expected, mRNA levels of myosin IIA/B
220 in L4/5 DRGs of *Advillin-Cre: myosin IIA/B*$^{f/f}$ mice were lowered (Figure 4A). Pearson correlation
221 coefficient of gene expression indicated by FPKM (Fragments Per Kilobase of exon model per Million
222 mapped reads) among different samples showed that under same treatment (sham or SNI), the two wild
223 type replicates were quite similar to the two dKO replicates (Figure 4B). When the numbers of
224 differentially expressed genes (DEGs) were compared, we found SNI significantly altered the mRNA
225 levels of nearly 2000 genes, whereas myosin IIA/B dKO caused little change. Specifically, the number of
226 DEGs between wild type neurons and myosin IIA/B dKO neurons was actually equivalent to that between
227 the two replicates within each condition (Figure 4C). These results indicated that myosin IIA/B dKO *per*
228 *se* did not significantly change the transcriptome in sensory neurons. In addition, in wild type and myosin
229 IIA/B dKO neurons we closely examined and compared the FPKMs of many classic regeneration-
230 associated genes (RAGs) and genes well-known to control axon regeneration, such as *Atf3*, *Sox11*, *Lin28a*,
231 *Gap43*, *Pten*, *Klf9*, and *Rab27*, etc[13,27-31]. The results showed that the mRNA levels of these genes were
232 up- or downregulated by SNI as expected, but were not largely affected by myosin IIA/B dKO (Figure
233 4D, E). Gene ontology analysis of DEGs between different conditions revealed that SNI stimulated many
234 neuron-related programs (Figure 4G), whereas myosin IIA/B dKO induced gene expression change had
235 no specific connection with neurons or axon regeneration (Figure 4H). Lastly, we directly examined the
236 protein levels of several genes and pathways regulating axon regeneration by western blot and found that
237 in either uninjured or injured condition, myosin IIA/B dKO did not change the protein levels of Atf3, c-
238 Jun, Gap43 or c-Myc (Figure 4F). Moreover, consistent with our RGC immunostaining results, myosin
239 IIA/B dKO had no impact on mTOR or GSK3β pathway (Figure 4F) in sensory neurons. Taken together,

240 these results further supported that myosin IIA/B dKO induced optic nerve regeneration was unlikely to
241 be caused by enhanced intrinsic axon regeneration ability.
242
243 **Knocking out non-muscle myosin IIA/B in RGCs changed axon tip morphology and regenerating**
244 **axon trajectory**
245 To better understand the cellular mechanisms by which myosin IIA/B knockout promoted optic
246 nerve regeneration, we first performed detailed analysis of axonal tip morphologies in wild type and
247 myosin IIA/B dKO optic nerves 2 and 4 weeks after ONC. Based on a previous study[32], there are mainly
248 three types of axonal tip morphologies in vivo. One is the retraction bulb (Figure 5A, C), which is the
249 hallmark structure of dystrophic axons that failed to regenerate[17,19]. The other two are growth-competent
250 growth cones with two different end shapes (Figure 5A, C). We found that in wild type optic nerves, a
251 significant percentage of axons had retraction bulbs at their ends, whereas knocking out myosin IIA/B in
252 RGCs almost abolished the formation of retraction bulbs (Figure 5A, B). Most regenerating axons in the
253 myosin IIA/B knockout nerves had growth-competent growth cones, indicating that deleting myosin IIA/B
254 efficiently transformed dystrophic axon tips into growth cones and rendered subsequent axon regeneration.
255 The tissue clearing and confocal imaging of whole-mount optic nerves allowed us to visualize the
256 bona fide morphology of regenerating axons. Thus, we next examined how myosin IIA/B knockout
257 influenced the axon extension trajectories 4 weeks after ONC. In wild type nerves, the majority of axons
258 followed a wandering path with many curves and backward turns (U-turns), which resulted in very
259 inefficient axon regeneration towards the distal optic nerve. In contrast, in myosin IIA/B dKO nerves,
260 most regenerating axons were straight with significantly reduced U-turns (Figure 5D-F and
261 Supplementary Figures 5, 6), indicating a higher efficiency of axon regeneration. Together, we think that
262 enhanced optic nerve regeneration induced by myosin IIA/B dKO was achieved through 1) switching

263 retraction bulbs into growth-competent growth cones, and 2) more efficient axon regeneration with
264 straighter axon growth and less U-turns.
265

266 **Discussion**

267 In addition to diminished intrinsic axon regeneration capacity regulated by changes in gene
268 expression during neuronal maturation, dystrophic growth cone with disruptive cytoskeletal dynamics is
269 another key intrinsic barrier for successful CNS axon regeneration[17]. Although it has been well recognized
270 that modulation of axonal cytoskeleton would be a plausible approach to enhance CNS axon regeneration,
271 very few studies have shown direct and convincing results. Two previous elegant studies[33,34] have shown
272 that moderate stabilization of microtubules with taxol or epothilone B could promote axon regeneration
273 after the spinal cord injury. The promoting effects were achieved through decreased glial scar formation,
274 which rendered the lesion site more permissive, and improved microtubule protrusion in the growth cones
275 of the injured axons. However, the promoting effects were moderate with regenerating axons only entering
276 the injury site. Similarly, after optic nerve injury low dose taxol treatment alone had little promoting effect
277 on axon regeneration [35]. In this study we provided clear and strong evidence that knocking out myosin
278 IIA/B in RGCs alone was sufficient to induce robust and sustained optic nerve regeneration. Based on our
279 previous in vitro study[20] we think that deleting myosin IIA/B acted locally at the growth cone without
280 affecting signaling events at the neuronal soma and gene transcription. Thus, we first examined two well-
281 known signaling pathways in RGCs, mTOR activation and GSK3β inactivation, which occur in the
282 neuronal soma to support the intrinsic axon regeneration ability. The results showed that deleting myosin
283 IIA/B had no effects on these two pathways, suggesting that the intrinsic axon regeneration ability of
284 RGCs might not be elevated. In contrast, overexpression of Lin28a, which promotes optic nerve
285 regeneration by enhancing the intrinsic axon regeneration ability, led to marked activation of mTOR and
286 inactivation of GSK3β in RGCs. Next, by using sensory neuron specific myosin IIA/B conditional
287 knockout mice, we explored how deleting myosin IIA/B affected sensory neuron transcriptome. The
288 results showed that deleting myosin IIA/B did not significantly change the transcription profile in sensory

289 neurons. More importantly, when the transcription levels of many known RAGs were examined, we found
290 that peripheral axotomy significantly changed their mRNA levels, whereas knocking out myosin IIA/B
291 had little effects. Lastly, we directly examined the protein levels of selected RAGs and signaling mediators
292 with western blot. Similarly, knocking out myosin IIA/B had little effects, whereas peripheral axotomy
293 showed significant impact. Collectively, these results provided strong and clear evidence that myosin
294 IIA/B knockout promoted optic nerve regeneration without affecting gene transcription and the intrinsic
295 axon regeneration ability.

296 To better understand how knocking out myosin IIA/B promoted optic nerve regeneration, we
297 carefully examined how RGC axonal morphology and trajectory were affected. The inability of mature
298 CNS axon to form a growth-competent growth cone in the inhibitory environment after injuries is a
299 hallmark of regeneration failure[17,19]. In most cases, after CNS injuries, a bulb-like structure is formed at
300 the tip of the injured axon, called the retraction bulb[32]. Indeed, very limited optic nerve regeneration was
301 observed in wild type mice, and retraction bulbs were often observed at the tips of the axons. In contrast,
302 in myosin IIA/B dKO nerves, very few retraction bulbs were identified, while growth-competent growth
303 cones could be found at almost all axonal tips, indicating that deleting myosin IIA/B was an efficient
304 strategy to transform retraction bulbs into growth cones. Based on our previous in vitro study[20], it is likely
305 achieved through slowed retrograde flow of actin filaments and the subsequent protrusion of microtubules
306 in the dystrophic growth cones. In addition, confocal microscopy of cleared whole-mount optic nerves
307 allowed us to trace the trajectories of regenerating axons. We found that in the wild type group, the
308 majority of axons showed wandering trajectories with many kinks and U-turns, likely due to the inhibitory
309 substrates in the optic nerve. As a result, such axon extension resulted in very inefficient axon regeneration.
310 When myosin IIA/B were knocked out, most axons followed a straighter path with reduced U-turns,
311 indicating overcoming inhibitory cues upon myosin IIA/B deletion and greatly enhanced regeneration

312 efficiency. Collectively, these results suggested that deleting myosin IIA/B promoted optic nerve
313 regeneration via efficiently transforming retraction bulbs into active growth cones and more efficient axon
314 extension within the inhibitory CNS environment.

315 Long-distance axon regeneration is one of the most important aspects and a prerequisite for
316 successful functional recovery after neural injuries. Several previous studies[36,37], including ours[13], have
317 shown that combined manipulation of multiple genes/pathways usually have additive promoting effects
318 on optic nerve regeneration. Here we showed that combining myosin IIA/B knockout with Lin28a
319 overexpression resulted in surprisingly long-distance optic nerve regeneration. Two weeks after ONC,
320 regenerating axon reached up to 3.25 mm from the crush site (nearly 4 mm in real distance considering
321 18% shrinkage due to tissue clearing process[13]) without enhancing the RGC survival rate. The longest
322 regenerating axons were about 4.3 mm and close to the optic chiasm. To our knowledge, such distance
323 was longer than most previous published studies using combinatory approaches. For instance, we recently
324 showed that combining Lin28a overexpression with Pten knocking down in RGCs resulted in optic nerve
325 regeneration up to 2.4 mm from the crush site 2 weeks after ONC[13]. In an earlier study[36], combined
326 knockout of Pten and SOCS3, together with CNTF, led to optic nerve regeneration up to 3 mm from the
327 crush site 2 weeks after ONC. Moreover, combining Zymosan, c-AMP, and Pten deletion could promote
328 optic nerve regeneration to 3 mm from the crush site[37]. The effectiveness of the combinatory approach
329 will be optimal if each gene/pathway acts independently. Indeed, Lin28a and myosin II acted in distinct
330 neuronal compartments with distinct cellular mechanisms, resulting in an optimized combination.
331 Although the number of long-distance regenerating axons observed in this study was relatively low, it was
332 likely due to the poor survival of RGCs as neither myosin IIA/B knockout (Figure 1D, E) nor Lin28a
333 overexpression[13] protects RGCs from dying after injury. Thus, future studies combining myosin II
334 knockout with other regeneration approaches, as well as enhanced RGC survival, would very likely lead

335 to large number of axons regenerating back to their original targets in the brain and gain recovery of lost
336 visual function. Moreover, the availability of water soluble and stable pharmacological inhibitor of myosin
337 II[38] would make future translational applications possible to repair axonal injuries induced by glaucoma,
338 spinal cord injury, traumatic brain injury, and neurodegenerative diseases.

339 **Methods**

340 **Mice**

341 All animal experiments were conducted in accordance with the protocol approved by the
342 Institutional Animal Care and Use Committee of the Johns Hopkins University. The *Myh9*$^{f/f}$
343 (stock#032096-UNC) and *Myh10*$^{f/f}$ (stock#016981-UNC) mouse strains were obtained from Mutant
344 Mouse Resource and Research Center (MMRRC) at University of North Carolina at Chapel Hill, an NIH-
345 funded strain repository, and were donated to the MMRRC by Robert S. Adelstein, M.D., National Heart,
346 Lung, and Blood Institute (NHLBI). The two lines were crossed to generate *Myh9*$^{f/f}$*: Myh10*$^{f/f}$ mice.
347 *Advillin-Cre* mouse line was a kind gift from Dr. Fan Wang's laboratory at Duke University, and was
348 crossed with *Myh9*$^{f/f}$*: Myh10*$^{f/f}$ to get *Advillin-Cre: Myh9*$^{f/f}$*: Myh10*$^{f/f}$ conditional knockout mice. The
349 tdTomato reporter line (stock#007909) was purchased from The Jackson Laboratory. Adult mice (6 weeks)
350 of both sexes were used. Genotypes of the mice were determined by PCR using primers provided by
351 MMRRC and The Jackson Laboratory. All animal surgeries were performed under anesthesia induced by
352 intraperitoneal injection of ketamine (100 mg/kg) and xylazine (10 mg/kg) diluted in sterile saline. Details
353 of the surgeries are described below.

354

355 **Construct**

356 The pAAV-Ef1a-Lin28a-FLAG plasmid was constructed in a previous study[13]. Briefly, the
357 Lin28a-FLAG open reading frame with a 5' BamHI and a 3' EcoRV restriction sites was synthesized
358 (codon optimized, gBlocks of Integrated DNA Technologies) and used for replacing the EYFP open
359 reading frame in pAAV-Ef1a-EYFP, to obtain the pAAV-Ef1a-Lin28a-FLAG plasmid. pAAV-Ef1a-
360 EYFP was a kind gift from Dr. Hongjun Song's laboratory at University of Pennsylvania. All restriction

361 enzymes and T4 DNA ligase were purchased from New England Biolabs. Plasmids were amplified using
362 DH5α competent cells (Thermo Fisher Scientific) and purified with Endofree plasmid maxi kit (Qiagen).
363

364 **Optic nerve regeneration model**

365 Intravitreal viral injection, optic nerve crush and RGC axon labeling were performed as previously
366 described[10]. Briefly, under anesthesia, 1.5 µl of AAV2 virus was injected into the right vitreous humor of
367 a mouse with a Hamilton syringe (32-gauge needle). The position and direction of the injection were well-
368 controlled to avoid injury to the lens. Two weeks later, the right optic nerve of the mouse was exposed
369 intraorbitally and crushed with Dumont #5 fine forceps (Fine Science Tools) for 5 s at approximately 1
370 mm behind the optic disc. To label RGC axons in the optic nerve, 1.5 µl of Alexa Fluor 594-conjugated
371 CTB (2 µg/µl, Thermo Fisher Scientific) was injected into the right vitreous humor with a Hamilton
372 syringe (32-gauge needle) 2 days before the mouse was sacrificed by transcardial perfusion under
373 anesthesia. The right optic nerve and bilateral retinas were dissected out and post-fixed in 4% PFA
374 overnight at 4°C. AAV2-Cre (SL100813) was purchased from SignaGen Laboratories. AAV2-Lin28a-
375 FLAG was also packaged by SignaGen Laboratories. All viruses used had titers over 1 x 10^{13} gc/ml.
376

377 **Optic nerve dehydration and clearing**

378 Dehydration and clearing of optic nerves were done based on previous studies[15,39]. Briefly, fixed
379 optic nerves were first dehydrated in increasing concentrations of tetrahydrofuran (50%, 70%, 80%, 100%
380 and 100%, v/v % in distilled water, 20 min each, Sigma-Aldrich) and then cleared in a solution of benzyl
381 alcohol and benzyl benzoate (BABB, 1:2, Sigma-Aldrich). Incubations were done on an orbital shaker at
382 room temperature. The nerves were stored in BABB in the dark at room temperature.
383

384 **Analysis of RGC axon regeneration**

385 Tissue cleared whole-mount optic nerves were imaged with a 20x objective on a Zeiss 800
386 confocal microscope. For each optic nerve, Z-stack and tiling (10% overlap) functions were used to
387 acquire stacked 2-µm-thick planes of the whole area of interest and the tiles were stitched.

388 To quantify the number of regenerating axons in each optic nerve, every 8 consecutive planes were
389 Z-projected (maximum intensity) to generate a series of Z-projection images of 16-µm-thick optical
390 sections. At each 250-µm interval from the crush site, the number of CTB-labeled axons was counted in
391 each Z-projection image and summed over all optical sections.

392 To quantify the average length of top 5 longest axons of each optic nerve, all stitched 2-µm-thick
393 planes were Z-projected (maximum intensity) to obtain a single Z-projection image of the nerve. Top 5
394 longest regenerating axons were manually traced from the axonal tips to the crush site using the Fiji
395 software (NIH) to acquire the lengths of the axons.

396

397 **Immunohistochemistry of whole-mount retinas**

398 Fixed retinas were first radially cut into a petal shape (4 incisions) and blocked with PBST (1%)
399 containing 10% goat serum for 1 hr at room temperature. The retinas were then sequentially stained with
400 primary antibodies overnight at 4°C, and corresponding Alexa Fluor-conjugated secondary antibodies
401 (1:500, Thermo Fisher Scientific) for 2 hr at room temperature. All antibodies were diluted with the
402 blocking buffer. Following each antibody incubation, the retinas were washed with PBST (0.3%) for 4
403 times (15 min each). After the last wash, the retinas were mounted onto slides with Fluoroshield (Sigma-
404 Aldrich). Fluorescent images of the flat-mounted retinas were acquired with a 20x objective on a Zeiss
405 800 confocal microscope.

406

407 **Analysis of RGC transduction rate**

408 To quantify RGC transduction rate, uninjured right retinas (no optic nerve crush) were taken from
409 transcardially perfused *Myh9*$^{f/f}$*: Myh10*$^{f/f}$ mice 2 weeks after intravitreal AAV2-Cre injection. The retinas
410 were stained with mouse anti-tubulin β3 (Tuj1, 1:500, BioLegend) and rabbit anti-Cre recombinase (1:100,
411 Cell Signaling Technology) antibodies following the steps mentioned above (see Immnunohistochemistry
412 of whole-mount retinas). Five to eight fields under 20x objective were randomly obtained from the
413 peripheral regions of each flat-mounted retina. For each mouse, RGC transduction rate was calculated by
414 dividing the total number of Cre^{+}/Tuj1^{+} cells in all fields by the total number of Tuj1^{+} cells in all fields.
415 Only cells in the ganglion cell layer were counted.

416

417 **Analysis of RGC survival rate**

418 To quantify RGC survival rate, C57Bl6/J and *Myh9*$^{f/f}$*: Myh10*$^{f/f}$ mice injected with AAV2-Cre were
419 transcardially perfused 2 weeks after optic nerve crush and both retinas of each mouse were collected. The
420 retinas were stained with mouse anti-tubulin β3 antibody (Tuj1, 1:500, BioLegend) following the steps
421 mentioned above (see Immnunohistochemistry of whole-mount retinas). Seven or eight fields under 20x
422 objective were randomly taken from the peripheral regions of each flat-mounted retina. For each mouse,
423 RGC survival rate was calculated by dividing the average number of Tuj1^{+} cells in one field in the injured
424 retina (right) by that in the uninjured retina (left). Only cells in the ganglion cell layer were counted.

425

426 **Immunohistochemistry of retinal sections**

427 Fixed retinas were sectioned with a cryostat (10 μm) and the retinal sections were warmed on a
428 slide warmer at 37°C for 1 hr. Sections were rinsed once in PBS, soaked in 100°C citrate buffer (pH 6)
429 for 15 min, let to cool in the buffer to room temperature and then washed twice (5 min each) in PBS. After

430 being blocked with PBST (0.3%) containing 10% goat serum at room temperature for 1 hr, the sections
431 were stained with primary antibodies against target molecules overnight at 4 °C, followed by
432 corresponding Alexa Fluor-conjugated secondary antibodies (1:500, Thermo Fisher Scientific) at room
433 temperature for 1 hr. All antibodies were diluted with the blocking buffer. The sections were washed for
434 4 times (5, 5, 10, 10 min) with PBST (0.3%) following each antibody incubation and finally mounted with
435 DAPI Fluoromount-G (SouthernBiotech). Fluorescent images of the retinal sections were taken with a
436 CCD camera connected to a Zeiss inverted fluorescence microscope controlled by AxioVision software.
437

438 **Analysis of myosin IIB level in RGCs**

439 To analyze myosin IIB level in RGCs, both retinas (uninjured) of each mouse were taken from
440 transcardially perfused *Myh9*$^{f/f}$*: Myh10*$^{f/f}$ mice 2 weeks after intravitreal AAV2-Cre injection and sectioned.
441 The retinal sections were stained with mouse anti-tubulin β3 (Tuj1, 1:500, BioLegend) and rabbit anti-
442 myosin IIB (1:100, Thermo Fisher Scientific) antibodies following the steps mentioned above (see
443 Immnunohistochemistry of retinal sections).

444 To quantify the fluorescence intensity of myosin IIB in all RGCs, at least 7 non-adjacent retinal
445 sections acquired with identical imaging configurations were analyzed for each retina. Fluorescence
446 intensity was measured using the "outline spline" function of AxioVision and the background fluorescence
447 intensity was subtracted.
448

449 **Analysis of S6 and GSK3β phosphorylation**

450 To analyze S6 and GSK3β phosphorylation in RGCs, C57Bl6/J and *Myh9*$^{f/f}$*: Myh10*$^{f/f}$ mice injected
451 with AAV2-Cre, and *Myh9*$^{f/f}$*: Myh10*$^{f/f}$ mice injected with AAV2-Lin28a-FLAG were transcardially
452 perfused 2 weeks after optic nerve crush and the right retina of each mouse was collected and sectioned.

453 The retinal sections were stained with mouse anti-tubulin β3 antibody (Tuj1, 1:500, BioLegend), and
454 rabbit anti-pS6 Ser235/236 (1:200, Cell Signaling Technology) or rabbit anti-pGSK3β Ser9 (1:200, Cell
455 Signaling Technology) antibody following the steps mentioned above (see Immnunohistochemistry of
456 retinal sections).

457 To quantify the percentage of $pS6^+$ or $pGSK3\beta^+$ RGCs, at least 363 or 434 RGCs from at least 7
458 non-adjacent retinal sections from each mouse were analyzed. For each mouse, the percentage of $pS6^+$ or
459 $pGSK3\beta^+$ RGCs was calculated by dividing the number of $pS6^+/Tuj1^+$ or $pGSK3\beta^+/Tuj1^+$ cells by the
460 number of $Tuj1^+$ cells. Only cells in the ganglion cell layer were counted.

461 The relative fluorescence intensity of each RGC was calculated by dividing the fluorescence
462 intensity of the RGC by that of its adjacent tissue. To quantify the fluorescence intensity of pS6 or pGSK3β
463 in all RGCs, 20 retinal sections acquired with identical imaging configurations from at least 2 mice were
464 analyzed for each group. To quantify the fluorescence intensity of pS6 or pGSK3β in S6-activated or
465 GSK3β-inactivated RGCs, at least 40 RGCs with identical imaging configurations from at least 2 mice
466 were analyzed for each group. Fluorescence intensity of RGCs were measured using the "outline spline"
467 function of AxioVision.

468

469 **Sciatic nerve injury model**

470 Under anesthesia, bilateral sciatic nerves of a mouse were exposed and axotomized right below
471 pelvis. Nerves were only exposed but not axotomized for a sham surgery. Three days after the surgery,
472 the mouse was euthanized and bilateral L4/5 DRGs were collected and used for total RNA or protein
473 extraction.

474

475 **mRNA sequencing and data analysis**

476 Total RNA was isolated with RNeasy mini kit (Qiagen) and RNA integrity was determined by
477 Agilent 2100 bioanalyzer and RNA 6000 Nano kit (Agilent Technologies). Paired-end libraries were
478 synthesized using the TruSeq RNA library preparation kit (Illumina). Briefly, mRNA molecules were
479 purified using oligo dT-attached magnetic beads. Following purification, the mRNA molecules were
480 fragmented into small pieces using divalent cations at 94°C for 8 min. The cleaved RNA fragments were
481 reversely transcribed into first strand cDNA using reverse transcriptase and random primers. This was
482 followed by second strand cDNA synthesis using DNA Polymerase I and RNase H. These cDNA
483 fragments then went through an end repair process, the addition of a single base, and the ligation of the
484 adapters. The products were then purified and enriched with PCR to obtain the final cDNA library.
485 Purified libraries were quantified by Qubit 2.0 fluorometer (Thermo Fisher Scientific) and validated by
486 Agilent 2100 bioanalyzer (Agilent Technologies) to confirm the insert size and calculate the mole
487 concentration. Cluster was generated by cBot with the library diluted to 10 pM and sequencing was done
488 on HiSeq 2500 (Illumina).

489 Sequencing raw reads were preprocessed by filtering out rRNA reads, sequencing adapters, short-
490 fragment reads and other low-quality reads using Seqtk (github.com/lh3/seqtk). Hisat2 (version 2.0.4)[40]
491 was used to map the cleaned reads to the mouse GRCm38.p4 (mm10) reference genome with two
492 mismatches. After genome mapping, Stringtie (version 1.3.0)[41,42] was run with a reference annotation to
493 generate FPKM (Fragments Per Kilobase of exon model per Million mapped reads) values for known
494 gene models[43]. Differentially expressed genes were identified using edgeR[44]. The *P* value significance
495 threshold in multiple tests was set by the false discovery rate (FDR)[45,46]. The cut-off for differentially
496 expressed genes was set as $P < 0.05$ and |log2fold change| > 1. For genes used for gene ontology (GO)
497 analyses, an additional cut-off of average FPKM > 1 in at least one condition was applied. GO analysis

498 was done using DAVID Bioinformatics Resources 6.8[47,48]. GO terms came from biological process,
499 cellular component and molecular function categories.
500
501 **Western blot analysis**
502 Total protein was extracted from L4/5 DRGs or retinas using the RIPA buffer containing protease
503 inhibitor cocktail (Sigma-Aldrich) and phosphatase inhibitor cocktail (Sigma-Aldrich). Identical amount
504 of total protein from each condition was then separated by 4-12% gradient SDS-PAGE gel electrophoresis
505 and transferred onto polyvinylidene fluoride membranes. After being blocked with TBST (1%) containing
506 5% blotting-grade blocker (Bio-Rad), the membranes were incubated overnight with primary antibodies
507 against target molecules at 4 °C, followed by corresponding HRP-linked secondary antibodies (1:2000,
508 Cell Signaling Technology) for 1 hr at room temperature. All antibodies were diluted with blocking buffer.
509 The membranes were washed with TBST (1%) for four times (5, 5, 10, 10 min) after each antibody
510 incubation. Rabbit primary antibodies against myosin IIA (1:1000), Gap43 (1:1000), c-Jun (1:1000), c-
511 Myc (1:1000), pAkt Ser473 (1:2000), pGSK3β Ser9 (1:1000), pS6 Ser235/236 (1:2000) were purchased
512 from Cell Signaling Technology. Mouse anti-Atf3 primary antibody (1:100) was from Santa Cruz
513 Biotechnology. Mouse anti-β-actin primary antibody (1:5000) was from Sigma-Aldrich.
514
515 **Analysis of axonal tip morphology**
516 The method was derived from a previous study[32]. For each optic nerve, top 10 longest axons were
517 first identified in the Z-projection image of the nerve. Then the maximum diameter of each axonal tip and
518 the diameter of the cylindrical shaft of the corresponding axon were measured using Fiji software (NIH),
519 and a tip/shaft ratio was calculated. An axonal tip was defined as a retraction bulb if its tip/shaft ratio was
520 over 4. Otherwise, it was defined as a growth cone.

521

522 **Analysis of axon extension efficiency**

523 For each optic nerve, a 250-μm-long region with equivalent number of axons in the Z-projection
524 image of the nerve was used for analysis. All traceable axons within this region were manually traced. For
525 each axon, the length (covered distance on its trajectory) and the displacement (distance along the
526 longitudinal axis of the nerve, sometimes could be zero or negative) between the start point and the end
527 point were measured using Fiji software (NIH). The extension efficiency of each nerve was calculated by
528 dividing the summed displacement by the summed length of all axons.

529

530 **Analysis of U-turn rate**

531 For each optic nerve, top 15 longest axons were identified in the Z-projection image of the nerve
532 and their trajectories near the axonal tips were traced. A U-turn was defined when the angle between the
533 final direction of the axonal tip and the positive longitudinal axis of the optic nerve was wider than 90
534 degrees. U-turn rate of each nerve was calculated by dividing the number of axons that made U-turns by
535 15.

536

537 **Quantification and statistical analysis**

538 Statistical analyses were done with GraphPad Prism 7 and the significance level was set as $P <$
539 0.05. Data are represented as mean ± SEM unless specifically stated. For comparisons between two groups,
540 two-tailed unpaired or paired t test was used. For comparisons among three or more groups, one-way
541 ANOVA followed by Tukey's multiple comparisons test was used to determine the statistical significance.
542 Fisher's exact test was used to test contingency tables. All details regarding statistical analyses, including
543 the tests used, *P* values, exact values of n, definitions of n, are described in figure legends.

544 **Data availability**

545 The data that support the findings of this study are available from the corresponding author upon
546 reasonable request. RNA-seq raw data will be deposited and accession code will be available before
547 publication.

548

549 **Acknowledgements:** We appreciate Dr. Michele Pucak's help in confocal imaging experiments and
550 analyses. The study was supported by grants (to F.Q.Z.) from NIH (R01NS064288, R01NS085176,
551 R01GM111514, R01EY027347), the Craig H. Neilsen Foundation (259450), and the BrightFocus
552 Foundation (G2017037). Saijilafu was supported by the grants from the National Natural Science
553 Foundation of China (81571189, 81772353), the National Key Research and Development Program
554 (2016YFC1100203), and Innovation and Entrepreneurship Program of Jiangsu Province.

555

556 **Author Contributions:** X.-W.W., S.-G.Y., S., and F.-Q.Z. conceived the study and designed the project;
557 X.-W.W. and S.-G.Y. performed most of the experiments; C.Z. performed and analyzed the
558 immunostaining experiments; Y.Z. analyzed optic nerve regeneration; C.Z. and Y.Z. analyzed the axon
559 morphologies and trajectories; J.-J.M. performed the sensory neuron RNA-seq experiment; Y.-L.W. and
560 G.-L.M. helped with the optic nerve regeneration experiments; B.-B.Y., and A.R.K. helped with the data
561 analyses; X.-W.W. and F.-Q.Z. wrote the manuscript with contribution from all authors.

562

563 **Competing interests:** The authors declare no competing interests.

564 **Reference:**

565 1 He, Z. & Jin, Y. Intrinsic Control of Axon Regeneration. *Neuron* **90**, 437-451,
566 doi:10.1016/j.neuron.2016.04.022 (2016).

567 2 Curcio, M. & Bradke, F. Axon Regeneration in the Central Nervous System: Facing the Challenges from
568 the Inside. *Annu Rev Cell Dev Biol* **34**, 495-521, doi:10.1146/annurev-cellbio-100617-062508 (2018).

569 3 David, S. & Aguayo, A. J. Axonal elongation into peripheral nervous system "bridges" after central nervous
570 system injury in adult rats. *Science* **214**, 931-933 (1981).

571 4 Fawcett, J. W. The Paper that Restarted Modern Central Nervous System Axon Regeneration Research.
572 *Trends Neurosci* **41**, 239-242, doi:10.1016/j.tins.2018.02.012 (2018).

573 5 Richardson, P. M., Mcguinness, U. M. & Aguayo, A. J. Axons from Cns Neurons Regenerate into Pns
574 Grafts. *Nature* **284**, 264-265, doi:DOI 10.1038/284264a0 (1980).

575 6 So, K. F. & Aguayo, A. J. Lengthy regrowth of cut axons from ganglion cells after peripheral nerve
576 transplantation into the retina of adult rats. *Brain Res* **328**, 349-354 (1985).

577 7 Geoffroy, C. G. & Zheng, B. Myelin-associated inhibitors in axonal growth after CNS injury. *Current*
578 *opinion in neurobiology* **27**, 31-38, doi:10.1016/j.conb.2014.02.012 (2014).

579 8 Lee, J. K. & Zheng, B. Role of myelin-associated inhibitors in axonal repair after spinal cord injury. *Exp*
580 *Neurol* **235**, 33-42, doi:10.1016/j.expneurol.2011.05.001 (2012).

581 9 Liu, K. *et al.* PTEN deletion enhances the regenerative ability of adult corticospinal neurons. *Nat Neurosci*
582 **13**, 1075-1081, doi:10.1038/nn.2603 (2010).

583 10 Park, K. K. *et al.* Promoting axon regeneration in the adult CNS by modulation of the PTEN/mTOR
584 pathway. *Science* **322**, 963-966, doi:10.1126/science.1161566 (2008).

585 11 Moore, D. L. *et al.* KLF family members regulate intrinsic axon regeneration ability. *Science* **326**, 298-301,
586 doi:10.1126/science.1175737 (2009).

587 12 Smith, P. D. *et al.* SOCS3 Deletion Promotes Optic Nerve Regeneration In Vivo. *Neuron* **64**, 617-623,
588 doi:10.1016/j.neuron.2009.11.021 (2009).

589 13 Wang, X. W. *et al.* Lin28 Signaling Supports Mammalian PNS and CNS Axon Regeneration. *Cell Rep* **24**,
590 2540-2552 e2546, doi:10.1016/j.celrep.2018.07.105 (2018).

591 14 Geoffroy, C. G., Hilton, B. J., Tetzlaff, W. & Zheng, B. Evidence for an Age-Dependent Decline in Axon
592 Regeneration in the Adult Mammalian Central Nervous System. *Cell Rep* **15**, 238-246,
593 doi:10.1016/j.celrep.2016.03.028 (2016).

594 15 Luo, X. *et al.* Three-dimensional evaluation of retinal ganglion cell axon regeneration and pathfinding in
595 whole mouse tissue after injury. *Exp Neurol* **247**, 653-662, doi:10.1016/j.expneurol.2013.03.001 (2013).

596 16 Pernet, V. *et al.* Misguidance and modulation of axonal regeneration by Stat3 and Rho/ROCK signaling in
597 the transparent optic nerve. *Cell Death Dis* **4**, e734, doi:10.1038/cddis.2013.266 (2013).

598 17 Blanquie, O. & Bradke, F. Cytoskeleton dynamics in axon regeneration. *Current opinion in neurobiology*
599 **51**, 60-69, doi:10.1016/j.conb.2018.02.024 (2018).

600 18 Hur, E. M. *et al.* GSK3 controls axon growth via CLASP-mediated regulation of growth cone microtubules.
601 *Genes Dev* **25**, 1968-1981, doi:10.1101/gad.17015911 (2011).

602 19 Hur, E. M., Saijilafu & Zhou, F. Q. Growing the growth cone: remodeling the cytoskeleton to promote axon
603 regeneration. *Trends in Neurosciences* **35**, 164-174, doi:10.1016/j.tins.2011.11.002 (2012).

604 20 Hur, E. M. *et al.* Engineering neuronal growth cones to promote axon regeneration over inhibitory
605 molecules. *Proc Natl Acad Sci U S A* **108**, 5057-5062, doi:10.1073/pnas.1011258108 (2011).

606 21 Guo, X., Snider, W. D. & Chen, B. GSK3beta regulates AKT-induced central nervous system axon
607 regeneration via an eIF2Bepsilon-dependent, mTORC1-independent pathway. *Elife* **5**, e11903,
608 doi:10.7554/eLife.11903 (2016).

609 22 Miao, L. *et al.* mTORC1 is necessary but mTORC2 and GSK3beta are inhibitory for AKT3-induced axon
610 regeneration in the central nervous system. *Elife* **5**, doi:10.7554/eLife.14908 (2016).

611 23 Duan, X. *et al.* Subtype-specific regeneration of retinal ganglion cells following axotomy: effects of
612 osteopontin and mTOR signaling. *Neuron* **85**, 1244-1256, doi:10.1016/j.neuron.2015.02.017 (2015).

613 24 Li, S. *et al.* Promoting axon regeneration in the adult CNS by modulation of the melanopsin/GPCR
614 signaling. *Proc Natl Acad Sci U S A* **113**, 1937-1942, doi:10.1073/pnas.1523645113 (2016).

615 25 Pita-Thomas, W., Mahar, M., Joshi, A., Gan, D. & Cavalli, V. HDAC5 promotes optic nerve regeneration
616 by activating the mTOR pathway. *Exp Neurol* **317**, 271-283, doi:10.1016/j.expneurol.2019.03.011 (2019).

617 26 Lim, J. H. *et al.* Neural activity promotes long-distance, target-specific regeneration of adult retinal axons.
618 *Nat Neurosci* **19**, 1073-1084, doi:10.1038/nn.4340 (2016).

619 27 Tsujino, H. *et al.* Activating transcription factor 3 (ATF3) induction by axotomy in sensory and
620 motoneurons: A novel neuronal marker of nerve injury. *Mol Cell Neurosci* **15**, 170-182, doi:DOI
621 10.1006/mcne.1999.0814 (2000).

622 28 Tanabe, K., Bonilla, I., Winkles, J. A. & Strittmatter, S. M. Fibroblast growth factor-inducible-14 is induced
623 in axotomized neurons and promotes neurite outgrowth. *Journal of Neuroscience* **23**, 9675-9686 (2003).

624 29 Christie, K. J., Webber, C. A., Martinez, J. A., Singh, B. & Zochodne, D. W. PTEN Inhibition to Facilitate
625 Intrinsic Regenerative Outgrowth of Adult Peripheral Axons. *Journal of Neuroscience* **30**, 9306-9315,
626 doi:10.1523/Jneurosci.6271-09.2010 (2010).

627 30 Apara, A. *et al.* KLF9 and JNK3 Interact to Suppress Axon Regeneration in the Adult CNS. *Journal of*
628 *Neuroscience* **37**, 9632-9644, doi:10.1523/Jneurosci.0643-16.2017 (2017).

629 31 Sekine, Y. *et al.* Functional Genome-wide Screen Identifies Pathways Restricting Central Nervous System
630 Axonal Regeneration. *Cell Reports* **23**, 415-428, doi:10.1016/j.celrep.2018.03.058 (2018).

631 32 Erturk, A., Hellal, F., Enes, J. & Bradke, F. Disorganized microtubules underlie the formation of retraction
632 bulbs and the failure of axonal regeneration. *J Neurosci* **27**, 9169-9180, doi:10.1523/JNEUROSCI.0612-
633 07.2007 (2007).

634 33 Hellal, F. *et al.* Microtubule Stabilization Reduces Scarring and Causes Axon Regeneration After Spinal
635 Cord Injury. *Science* **331**, 928-931, doi:10.1126/science.1201148 (2011).

636 34 Ruschel, J. *et al.* Axonal regeneration. Systemic administration of epothilone B promotes axon regeneration
637 after spinal cord injury. *Science* **348**, 347-352, doi:10.1126/science.aaa2958 (2015).

638 35 Sengottuvel, V., Leibinger, M., Pfreimer, M., Andreadaki, A. & Fischer, D. Taxol facilitates axon
639 regeneration in the mature CNS. *J Neurosci* **31**, 2688-2699, doi:10.1523/JNEUROSCI.4885-10.2011
640 (2011).

641 36 Sun, F. *et al.* Sustained axon regeneration induced by co-deletion of PTEN and SOCS3. *Nature* **480**, 372-
642 375, doi:10.1038/nature10594 (2011).

643 37 Kurimoto, T. *et al.* Long-distance axon regeneration in the mature optic nerve: contributions of
644 oncomodulin, cAMP, and pten gene deletion. *The Journal of neuroscience : the official journal of the*
645 *Society for Neuroscience* **30**, 15654-15663, doi:10.1523/JNEUROSCI.4340-10.2010 (2010).

646 38 Varkuti, B. H. *et al.* A highly soluble, non-phototoxic, non-fluorescent blebbistatin derivative. *Sci Rep* **6**,
647 26141, doi:10.1038/srep26141 (2016).

648 39 Erturk, A. *et al.* Three-dimensional imaging of solvent-cleared organs using 3DISCO. *Nat Protoc* **7**, 1983-
649 1995, doi:10.1038/nprot.2012.119 (2012).

650 40 Kim, D., Langmead, B. & Salzberg, S. L. HISAT: a fast spliced aligner with low memory requirements.
651 *Nat Methods* **12**, 357-360, doi:10.1038/nmeth.3317 (2015).

652 41 Pertea, M. *et al.* StringTie enables improved reconstruction of a transcriptome from RNA-seq reads. *Nat*
653 *Biotechnol* **33**, 290-295, doi:10.1038/nbt.3122 (2015).

654 42 Pertea, M., Kim, D., Pertea, G. M., Leek, J. T. & Salzberg, S. L. Transcript-level expression analysis of
655 RNA-seq experiments with HISAT, StringTie and Ballgown. *Nat Protoc* **11**, 1650-1667,
656 doi:10.1038/nprot.2016.095 (2016).

657 43 Mortazavi, A., Williams, B. A., McCue, K., Schaeffer, L. & Wold, B. Mapping and quantifying mammalian
658 transcriptomes by RNA-Seq. *Nat Methods* **5**, 621-628, doi:10.1038/nmeth.1226 (2008).

659 44 Robinson, M. D., McCarthy, D. J. & Smyth, G. K. edgeR: a Bioconductor package for differential
660 expression analysis of digital gene expression data. *Bioinformatics* **26**, 139-140,
661 doi:10.1093/bioinformatics/btp616 (2010).

662 45 Benjamini, Y. & Hochberg, Y. Controlling the False Discovery Rate - a Practical and Powerful Approach
663 to Multiple Testing. *J R Stat Soc B* **57**, 289-300 (1995).

664 46 Benjamini, Y. & Yekutieli, D. The control of the false discovery rate in multiple testing under dependency.
665 *Ann Stat* **29**, 1165-1188 (2001).

666 47 Huang, D. W., Sherman, B. T. & Lempicki, R. A. Systematic and integrative analysis of large gene lists
667 using DAVID bioinformatics resources. *Nature Protocols* **4**, 44-57, doi:10.1038/nprot.2008.211 (2009).

668 48 Huang, D. W., Sherman, B. T. & Lempicki, R. A. Bioinformatics enrichment tools: paths toward the
669 comprehensive functional analysis of large gene lists. *Nucleic Acids Research* **37**, 1-13,
670 doi:10.1093/nar/gkn923 (2009).

671

Figure 1

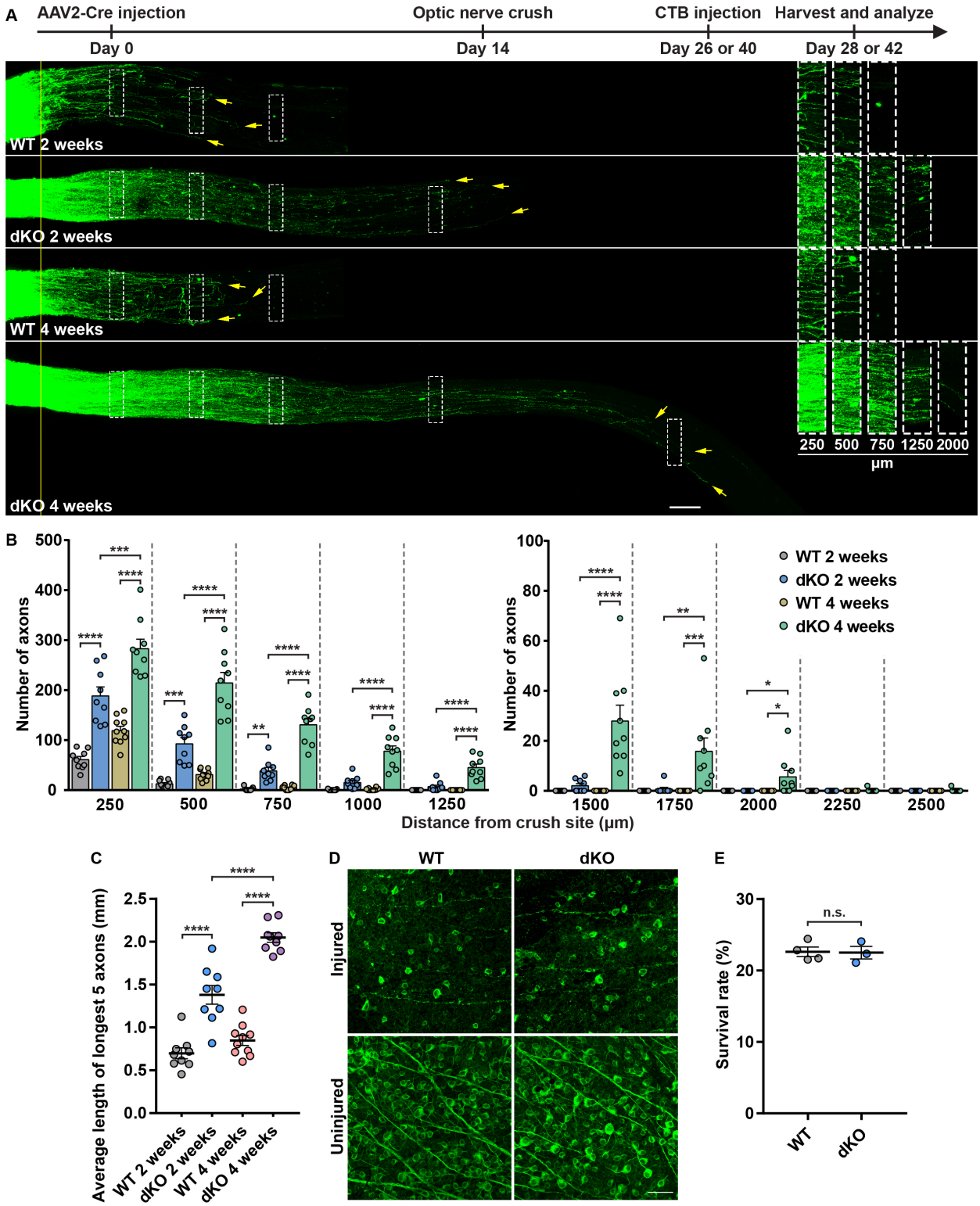
A
AAV2-Cre injection
Optic nerve crush
CTB injection
Harvest and analyze
Day 0
Day 14
Day 26 or 40
Day 28 or 42
WT 2 weeks
dKO 2 weeks
WT 4 weeks
dKO 4 weeks
250 500 750 1250 2000
μm
B
Number of axons
Distance from crush site (μm)
WT 2 weeks
dKO 2 weeks
WT 4 weeks
dKO 4 weeks
C
Average length of longest 5 axons (mm)
WT 2 weeks
dKO 2 weeks
WT 4 weeks
dKO 4 weeks
D
WT
dKO
Injured
Uninjured
E
Survival rate (%)
n.s.
WT
dKO

Figure 1. Deletion of myosin IIA/B in RGCs induced robust and sustained optic nerve regeneration.

(A) Top: experimental timeline. Bottom: representative images of optic nerves showing that deletion of myosin IIA/B in RGCs produced robust and persistent axon regeneration 2 and 4 weeks after optic nerve crush. The columns on the right display magnified images of the areas in white dashed boxes on the left, showing axons at 250, 500, 750, 1250 and 2000 μm distal to the crush sites. The yellow line indicates the crush sites. Yellow arrows indicate top 3 longest axons of each nerve. Scale bar, 100 μm (50 μm for the magnified images).

(B) Quantification of optic nerve regeneration in (A) (one-way ANOVA followed by Tukey's multiple comparisons test, $P < 0.0001$ at 250, 500, 750, 1000, 1250 and 1500 μm, $P = 0.0002$, 0.0071, 0.3875 and 0.3875 at 1750, 2000, 2250 and 2500 μm, respectively; n = 10 mice in 4-week WT group, n = 9 mice in other groups).

(C) Quantification of average length of top 5 longest axons of each nerve in (A) (one-way ANOVA followed by Tukey's multiple comparisons test, $P < 0.0001$; n = 10 mice in 4-week WT group, n = 9 mice in other groups).

(D) Representative images of flat-mounted retinas showing that deletion of myosin IIA/B had no effect on RGC survival rate 2 weeks after optic nerve crush. Flat-mounted retinas were stained with anti-tubulin β3 antibody (Tuj1, green). Scale bar, 50 μm.

(E) Quantification of RGC survival rate in (D) (unpaired t test, $P = 0.9092$, n = 4 and 3 mice in WT and dKO groups, respectively, 7-8 fields were analyzed for each retina).

Data are represented as mean ± SEM. n.s., not significant, *$P < 0.05$, **$P < 0.01$, ***$P < 0.001$, ****$P < 0.0001$. WT, wild type; dKO, double knockout of myosin IIA/B.

Figure 2

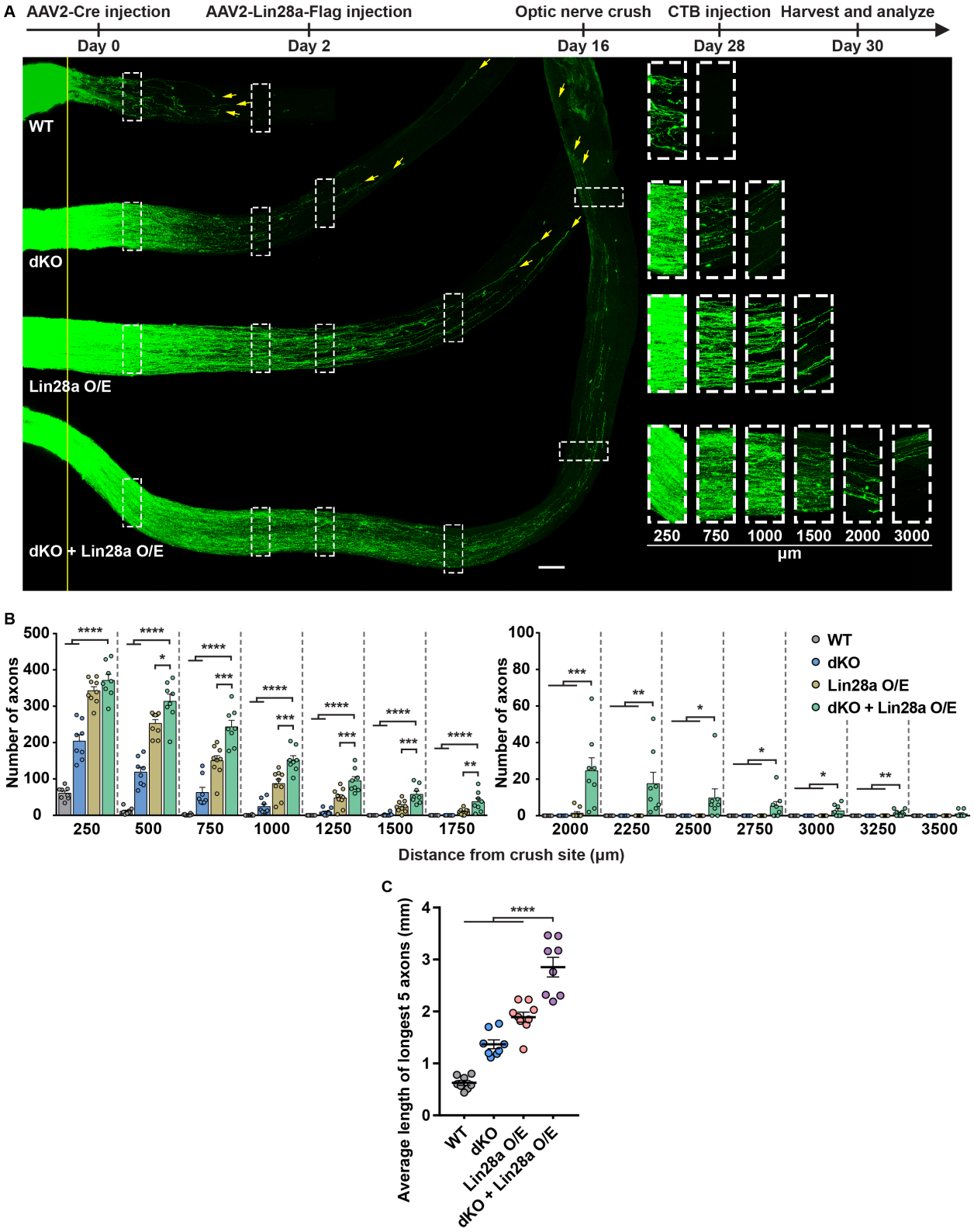
A
AAV2-Cre injection
AAV2-Lin28a-Flag injection
Optic nerve crush
CTB injection
Harvest and analyze
Day 0
Day 2
Day 16
Day 28
Day 30
WT
dKO
Lin28a O/E
dKO + Lin28a O/E
250
750
1000
1500
2000
3000
μm
B
Number of axons
Distance from crush site (μm)
WT
dKO
Lin28a O/E
dKO + Lin28a O/E
C
Average length of longest 5 axons (mm)
WT
dKO
Lin28a O/E
dKO + Lin28a O/E

Figure 2. Myosin IIA/B deletion and Lin28a overexpression had synergistic effect on optic nerve regeneration.

(A) Top: experimental timeline. Bottom: representative images of optic nerves showing that combined myosin IIA/B deletion and Lin28a overexpression in RGCs produced much stronger axon regeneration 2 weeks after the optic nerve crush. The columns on the right display magnified images of the areas in white dashed boxes on the left, showing axons at 250, 750, 1000, 1500, 2000 and 3000 μm distal to the crush sites. The yellow line indicates the crush sites. Yellow arrows indicate top 3 longest axons of each nerve. Scale bar, 100 μm (50 μm for the magnified images).

(B) Quantification of optic nerve regeneration in (A) (one-way ANOVA followed by Tukey's multiple comparisons test, $P < 0.0001$ at 250, 500, 750, 1000, 1250, 1500, 1750 and 2000 μm, $P = 0.0004$, 0.0206, 0.0092, 0.0042, 0.0026, 0.0844 at 2250, 2500, 2750, 3000, 3250 and 3500 μm, respectively; n = 9 mice in Lin28a O/E group, n = 8 mice in other groups).

(C) Quantification of average length of top 5 longest axons of each nerve in (A) (one-way ANOVA followed by Tukey's multiple comparisons test, $P < 0.0001$; n = 9 mice in Lin28a O/E group, n = 8 mice in other groups).

Data are represented as mean ± SEM. n.s., not significant, *$P < 0.05$, **$P < 0.01$, ***$P < 0.001$, ****$P < 0.0001$. WT, wild type; dKO, double knockout of myosin IIA/B; O/E, overexpression.

Figure 3

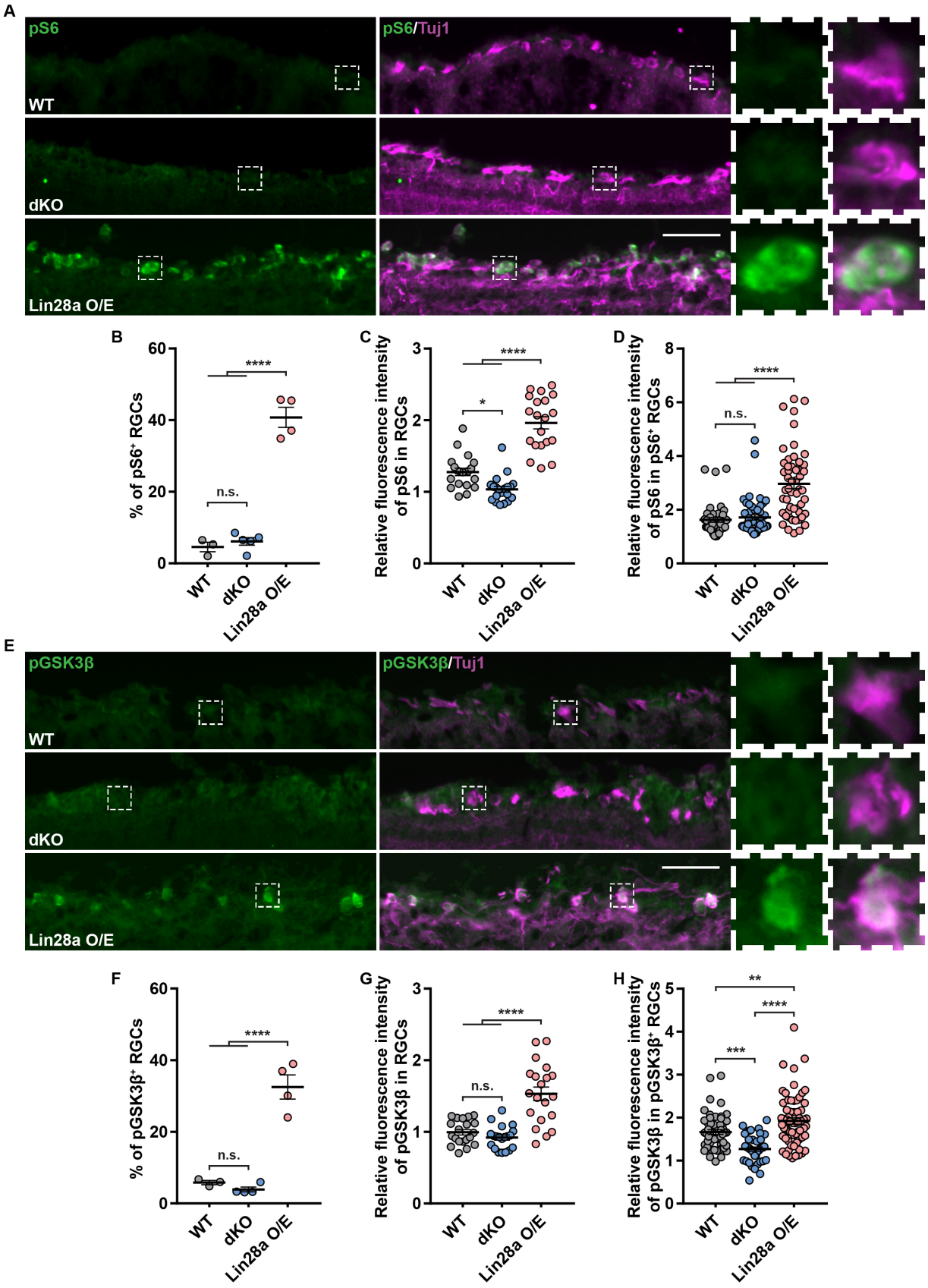
A
pS6
pS6/Tuj1
WT
dKO
Lin28a O/E
B
% of pS6+ RGCs
n.s.
****
WT
dKO
Lin28a O/E
C
Relative fluorescence intensity of pS6 in RGCs
*
****
D
Relative fluorescence intensity of pS6 in pS6+ RGCs
n.s.
****
E
pGSK3β
pGSK3β/Tuj1
F
% of pGSK3β+ RGCs
G
Relative fluorescence intensity of pGSK3β in RGCs
H
Relative fluorescence intensity of pGSK3β in pGSK3β+ RGCs
**
***

Figure 3. Myosin IIA/B deletion-induced optic nerve regeneration was independent of mTOR or GSK3β pathway.

(A) Representative images of retinal sections showing that deletion of myosin IIA/B did not activate mTOR (marked by pS6) in RGCs, whereas Lin28a overexpression markedly activated mTOR in RGCs 2 weeks after optic nerve crush. The two columns on the right display magnified images of the RGCs marked in white dashed boxes on the left. Retinal sections were stained with anti-pS6 (green) and anti-tubulin β3 (magenta) antibodies. Scale bar, 50 μm (12.5 μm for the magnified images).

(B) Quantification of the percentage of $pS6^+$ RGCs in (A) (one-way ANOVA followed by Tukey's multiple comparisons, $P < 0.0001$, n = 3 mice in WT group, n = 5 mice in dKO group, n = 4 mice in Lin28a O/E group, at least 363 RGCs from at least 7 non-adjacent retinal sections were analyzed for each mouse).

(C) Quantification of average fluorescence intensity of pS6 in all RGCs (one-way ANOVA followed by Tukey's multiple comparisons, $P < 0.0001$, n = 20 retinal sections with identical imaging configurations from at least 2 mice were analyzed for each group).

(D) Quantification of average fluorescence intensity of pS6 in $pS6^+$ RGCs (one-way ANOVA followed by Tukey's multiple comparisons, $P < 0.0001$, n = 42, 49 and 53 RGCs with identical imaging configurations from at least 2 mice were analyzed for WT, dKO and Lin28a O/E groups, respectively).

(E) Representative images of retinal sections showing that deletion of myosin IIA/B did not inactivate GSK3β (marked by pGSK3β) in RGCs, whereas Lin28a overexpression markedly inactivated GSK3β in RGCs 2 weeks after optic nerve crush. The right two columns display magnified images of the RGCs marked in white dashed boxes on the left. Retinal sections were stained with anti-pGSK3β (green) and anti-tubulin β3 (magenta) antibodies. Scale bar, 50 μm (12.5 μm for the magnified images).

(F) Quantification of the percentage of $pGSK3\beta^+$ RGCs in (E) (one-way ANOVA followed by Tukey's multiple comparisons, $P < 0.0001$, n = 3 mice in WT group, n = 4 mice in other groups, at least 434 RGCs from at least 7 non-adjacent retinal sections were analyzed for each mouse).

(G) Quantification of average fluorescence intensity of pGSK3β in all RGCs (one-way ANOVA followed by Tukey's multiple comparisons, $P < 0.0001$, n = 20 retinal sections with identical imaging configurations from at least 2 mice were analyzed for each group).

(H) Quantification of average fluorescence intensity of pGSK3β in $pGSK3\beta^+$ RGCs (one-way ANOVA followed by Tukey's multiple comparisons, $P < 0.0001$, n = 54, 40 and 65 RGCs with identical imaging configurations from at least 2 mice were analyzed for WT, dKO and Lin28a O/E groups, respectively).

Data are represented as mean ± SEM. n.s., not significant, $*P < 0.05$, $**P < 0.01$, $***P < 0.001$, $****P < 0.0001$. WT, wild type; dKO, double knockout of myosin IIA/B; O/E, overexpression.

Figure 4

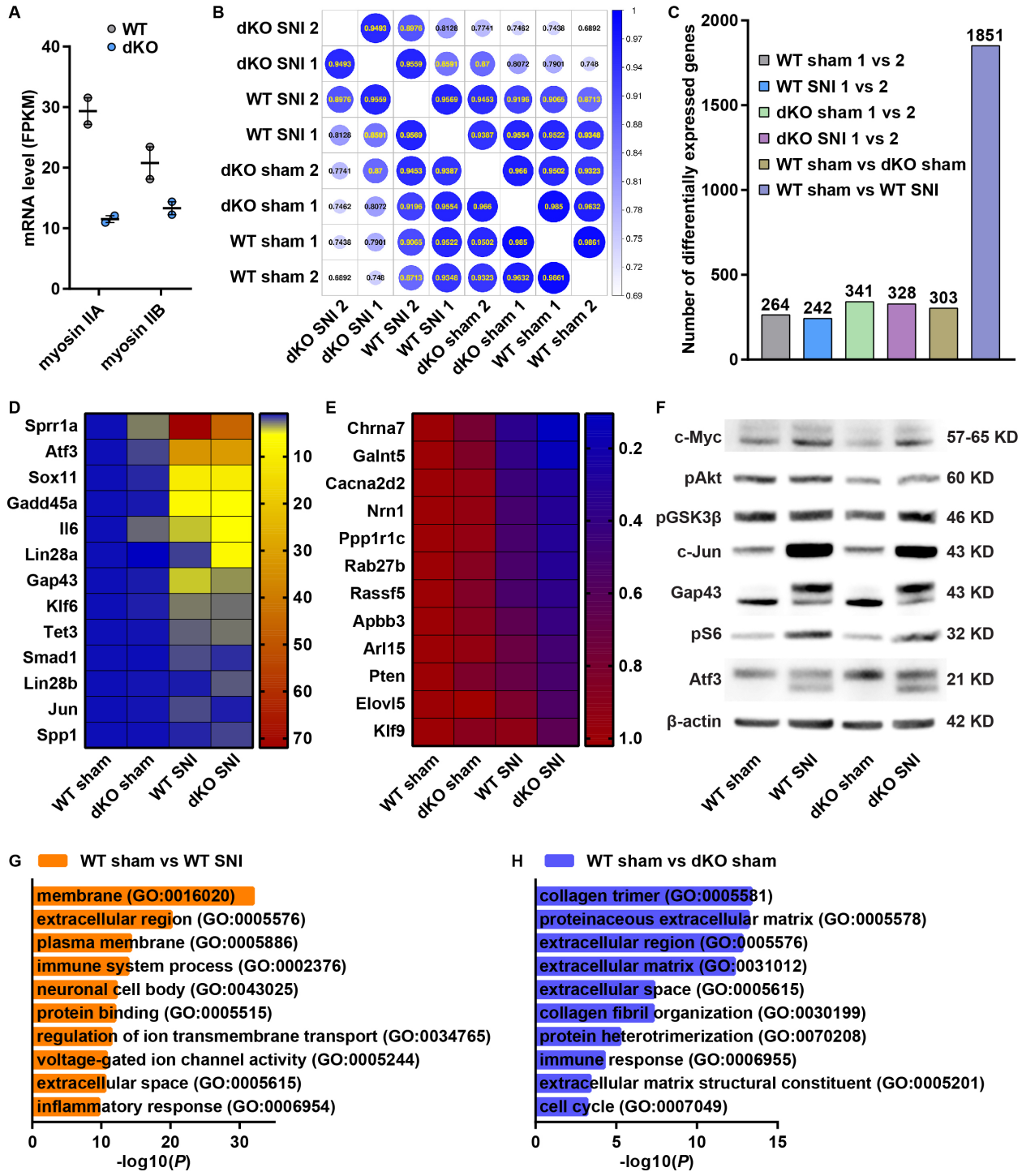
A
WT
dKO
mRNA level (FPKM)
myosin IIA
myosin IIB
B
dKO SNI 2
dKO SNI 1
WT SNI 2
WT SNI 1
dKO sham 2
dKO sham 1
WT sham 1
WT sham 2
C
Number of differentially expressed genes
WT sham 1 vs 2
WT SNI 1 vs 2
dKO sham 1 vs 2
dKO SNI 1 vs 2
WT sham vs dKO sham
WT sham vs WT SNI
264
242
341
328
303
1851
D
Sprr1a
Atf3
Sox11
Gadd45a
Il6
Lin28a
Gap43
Klf6
Tet3
Smad1
Lin28b
Jun
Spp1
WT sham
dKO sham
WT SNI
dKO SNI
E
Chrna7
Galnt5
Cacna2d2
Nrn1
Ppp1r1c
Rab27b
Rassf5
Apbb3
Arl15
Pten
Elovl5
Klf9
F
c-Myc
pAkt
pGSK3β
c-Jun
Gap43
pS6
Atf3
β-actin
57-65 KD
60 KD
46 KD
43 KD
43 KD
32 KD
21 KD
42 KD
G
WT sham vs WT SNI
membrane (GO:0016020)
extracellular region (GO:0005576)
plasma membrane (GO:0005886)
immune system process (GO:0002376)
neuronal cell body (GO:0043025)
protein binding (GO:0005515)
regulation of ion transmembrane transport (GO:0034765)
voltage-gated ion channel activity (GO:0005244)
extracellular space (GO:0005615)
inflammatory response (GO:0006954)
-log10(P)
H
WT sham vs dKO sham
collagen trimer (GO:0005581)
proteinaceous extracellular matrix (GO:0005578)
extracellular region (GO:0005576)
extracellular matrix (GO:0031012)
extracellular space (GO:0005615)
collagen fibril organization (GO:0030199)
protein heterotrimerization (GO:0070208)
immune response (GO:0006955)
extracellular matrix structural constituent (GO:0005201)
cell cycle (GO:0007049)
-log10(P)

Figure 4. Conditional knockout of myosin IIA/B in sensory neurons did not significantly affect known regeneration associated genes and pathways

(A) Decreased mRNA levels of myosin IIA/B in L4/5 DRGs of *Advillin-Cre: myosin IIA/B*$^{f/f}$ mice (n = 2 mice in each group, data are represented as mean ± SEM).

(B) Pearson correlation heatmap showing the high degree of similarity in gene transcription between wild type and myosin IIA/B deleted neurons under same condition (sham or SNI).

(C) Number of differentially expressed genes between replicates or conditions showing that myosin IIA/B deletion did not significantly change gene expression in neurons.

(D, E) Expression heatmap of genes known to be upregulated (D) or downregulated (E) following SNI. Results showed that myosin IIA/B deletion did not affect the transcription of these genes in neurons.

(F) Representative western blot results showing that neuron specific myosin IIA/B conditional knockout did not affect classic regeneration associated genes or pathways (n = 2 independent experiments).

(G, H) Gene ontology analyses of differentially expressed genes between uninjured (sham) and injured (SNI) condition in wild type neurons (G), and between wild type neurons and myosin IIA/B deleted neurons under uninjured (sham) condition (H).

WT, wild type. dKO, double knockout of myosin IIA/B. SNI, sciatic nerve injury.

Figure 5

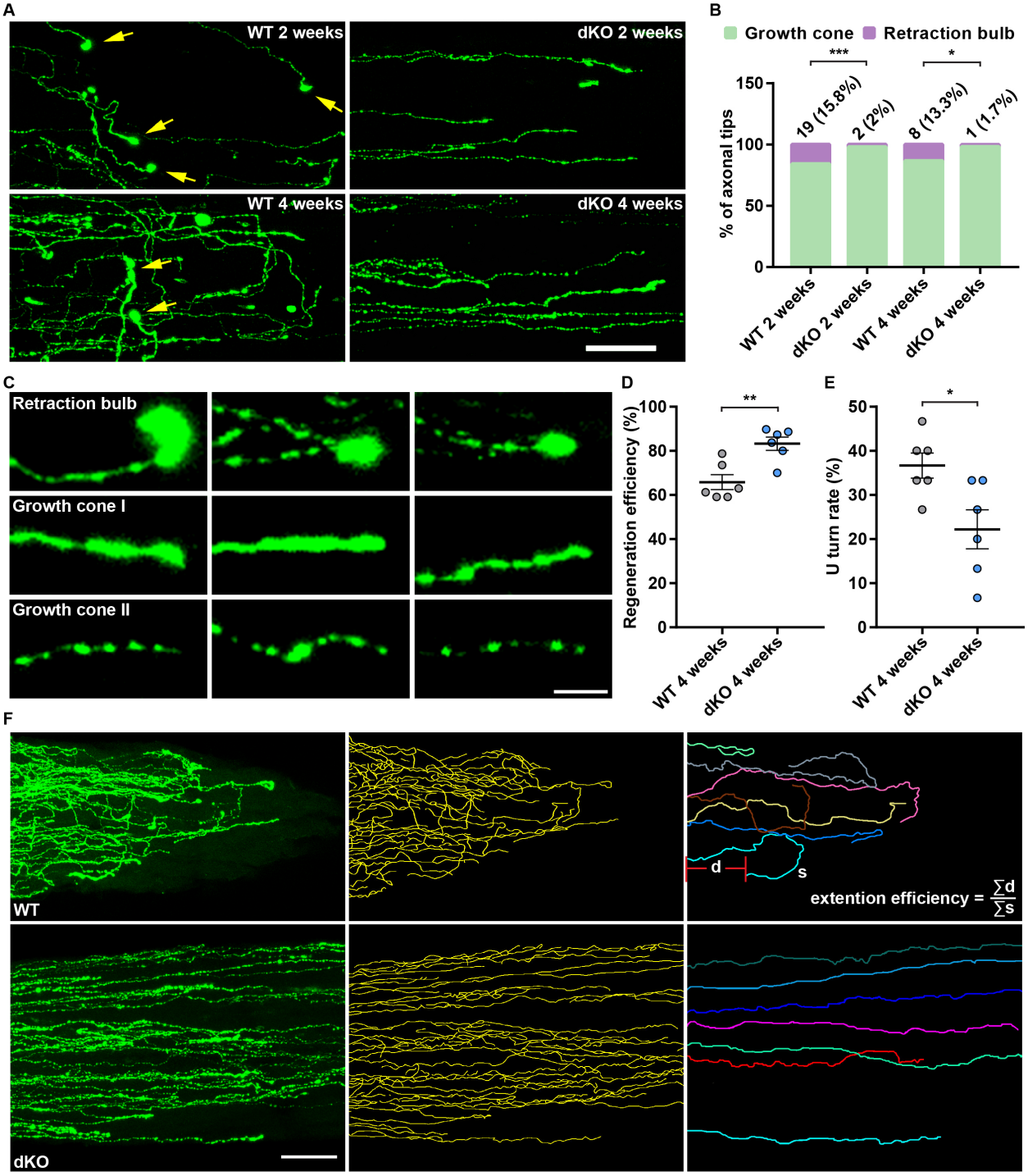
A
WT 2 weeks
dKO 2 weeks
WT 4 weeks
dKO 4 weeks
B
Growth cone
Retraction bulb
***
*
% of axonal tips
150
100
50
0
19 (15.8%)
2 (2%)
8 (13.3%)
1 (1.7%)
WT 2 weeks
dKO 2 weeks
WT 4 weeks
dKO 4 weeks
C
Retraction bulb
Growth cone I
Growth cone II
D
**
Regeneration efficiency (%)
100
80
60
40
20
0
WT 4 weeks
dKO 4 weeks
E
*
U turn rate (%)
50
40
30
20
10
0
WT 4 weeks
dKO 4 weeks
F
WT
d
s
extention efficiency = ∑d / ∑s
dKO

Figure 5. Myosin IIA/B deletion modified cytoskeletal dynamics to promote axon regeneration.

(A) Representative images of optic nerves showing that deletion of myosin IIA/B in RGCs abolished formation of retraction bulbs in optic nerves 2 and 4 weeks after optic nerve crush. Yellow arrows indicate retraction bulbs. Scale bar, 50 μm.

(B) Quantification of retraction bulbs in (A) (Fisher's exact test, $P = 0.0004$ and 0.0322 for 2 weeks and 4 weeks after optic nerve crush, respectively; n = 120 and 100 axonal tips from 12 nerves in 2-week WT and 10 nerves in dKO groups, respectively, n = 60 axonal tips from 6 nerves in each 4-week group).

(C) Representative images of retraction bulbs and growth cones found in different optic nerves. Scale bar, 5 μm.

(D) Quantification of axon extension efficiency in (F) and Figure S5 (unpaired t test, $P = 0.0032$, n = 6 mice in each group, at least 35 axons were analyzed for each mouse).

(E) Quantification of U-turn rate in Figure S6 (unpaired t test, $P = 0.0210$, n = 6 mice in each group, top 15 longest axons were analyzed for each mouse).

(F) Left: representative images of optic nerves showing that deletion of myosin IIA/B in RGCs improved axon extension efficiency 4 weeks after optic nerve crush. Middle: sketches of all axon traces in the left column. Right: detailed trajectories of a few axons (each color represents a single axon) in the left column. As illustrated, the extension efficiency of each nerve was calculated by dividing the summed displacement by the summed length of all traced axons. Scale bar, 50 μm.

Data are represented as mean ± SEM. *$P < 0.05$, **$P < 0.01$, ***$P < 0.001$. WT, wild type; dKO, double knockout of myosin IIA/B.

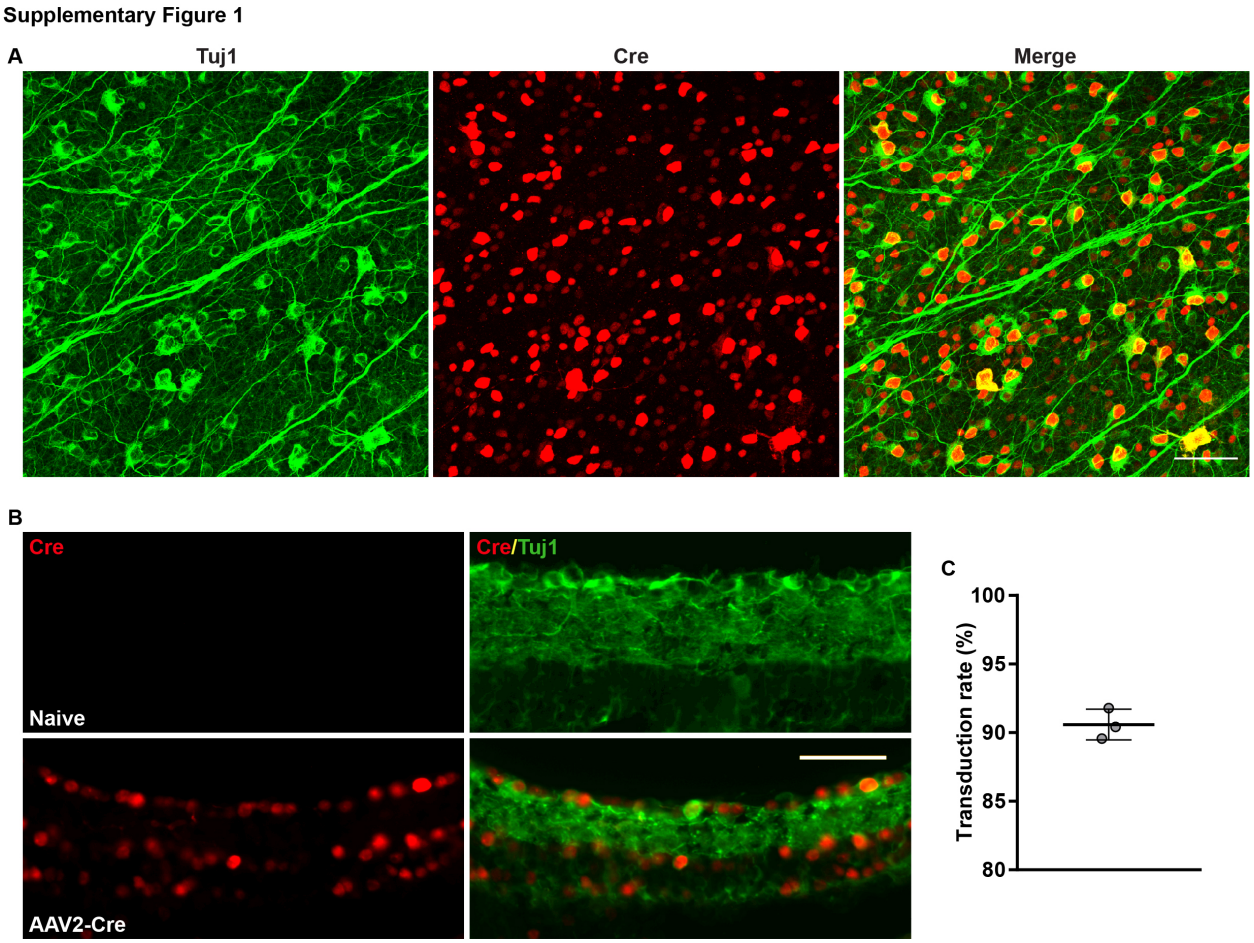

Supplementary Figure 1. Transduction rate of AAV2-Cre. Related to Figure 1.

(A) Representative images of flat-mounted retinas showing the high transduction rate of AAV2-Cre in RGCs. Flat-mounted retinas were stained with anti-tubulin β3 (Tuj1, green) and anti-Cre recombinase (red) antibodies. Scale bar, 50 μm.

(B) Representative images of retinal sections verifying the specificity of the anti-Cre antibody and the high transduction rate of AAV2-Cre in RGCs. Retinal sections were stained with anti-tubulin β3 (Tuj1, green) and anti-Cre (red) antibodies. Scale bar, 50 μm.

(C) Quantification of the transduction rate of AAV2-Cre in RGCs in (A). The average transduction rate is 90.59 ± 1.114% (n = 3 mice, 5-8 fields were analyzed for each mouse, data are represented as mean ± SD).

Supplementary Figure 2

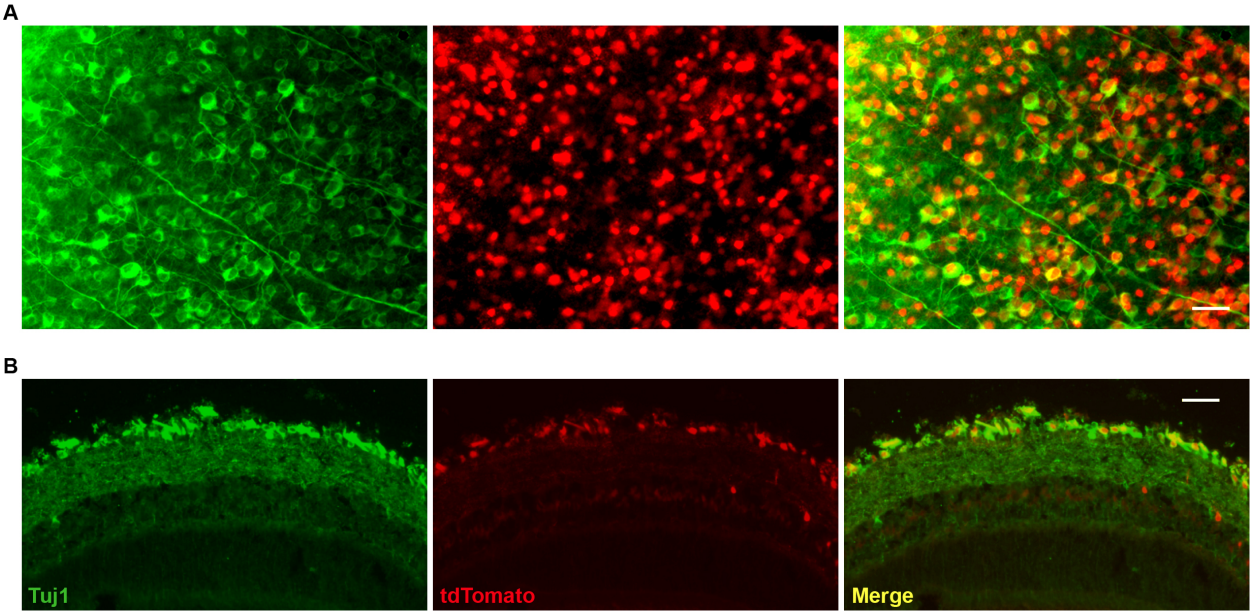

Supplementary Figure 2. Verification of the Cre-mediated gene recombination. Related to Figure 1.

(A, B) Representative images of flat-mounted retinas (A) and retinal sections (B) showing the expression of tdTomato in RGCs of tdTomato reporter mice, indicating successful Cre-mediated gene recombination 2 weeks after intravitreal AAV2-Cre injection. Flat-mounted retinas and retinal sections were stained with anti-tubulin β3 (Tuj1, green). Scale bar, 50 μm.

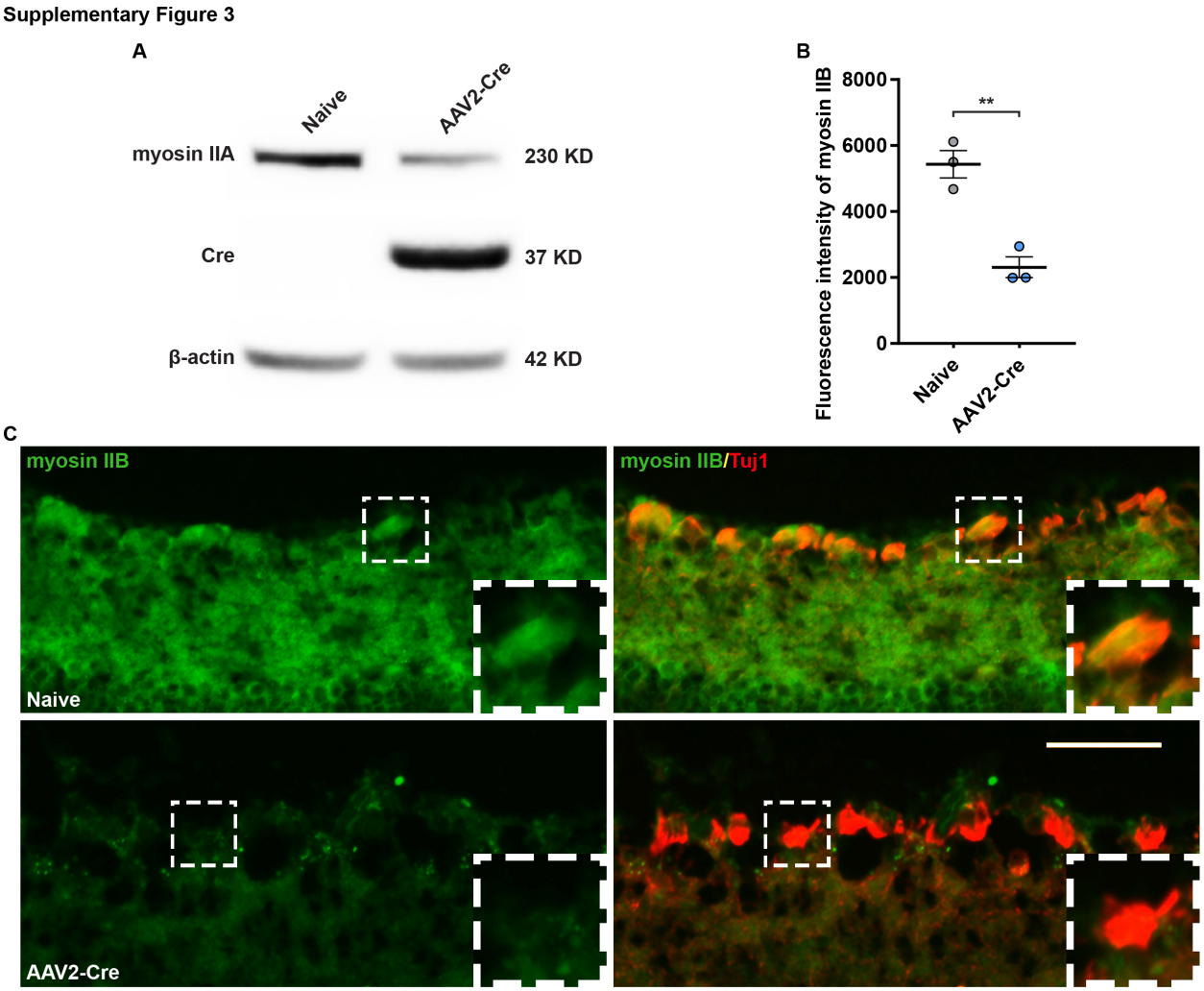

Supplementary Figure 3. Verification of myosin IIA/B deletion. Related to Figure 1.

(A) Western blot result showing the decreased protein level of myosin IIA in retina of a *myosin IIA/B*$^{f/f}$ mouse 2 weeks after intraviteal AAV2-Cre injection.

(B) Quantification of average fluorescence intensity of myosin IIB in (C) (paired t test, $P = 0.0057$, n = 3 mice, data are represented as mean ± SEM, $^{**}P < 0.01$, all images were taken with identical configurations).

(C) Representative images of retinal sections from the naïve (top) or the AAV2-Cre injected retina (bottom) of a *myosin IIA/B*$^{f/f}$ mouse showing the successful deletion of myosin IIB in RGCs 2 weeks after intravitreal AAV2-Cre injection. The insets display magnified images of the RGCs marked in white dashed boxes. Retinal sections were stained with anti-tubulin β3 (Tuj1, red) and anti-myosin IIB (green) antibodies. Scale bar, 50 µm (25 µm for the magnified images).

Supplementary Figure 4

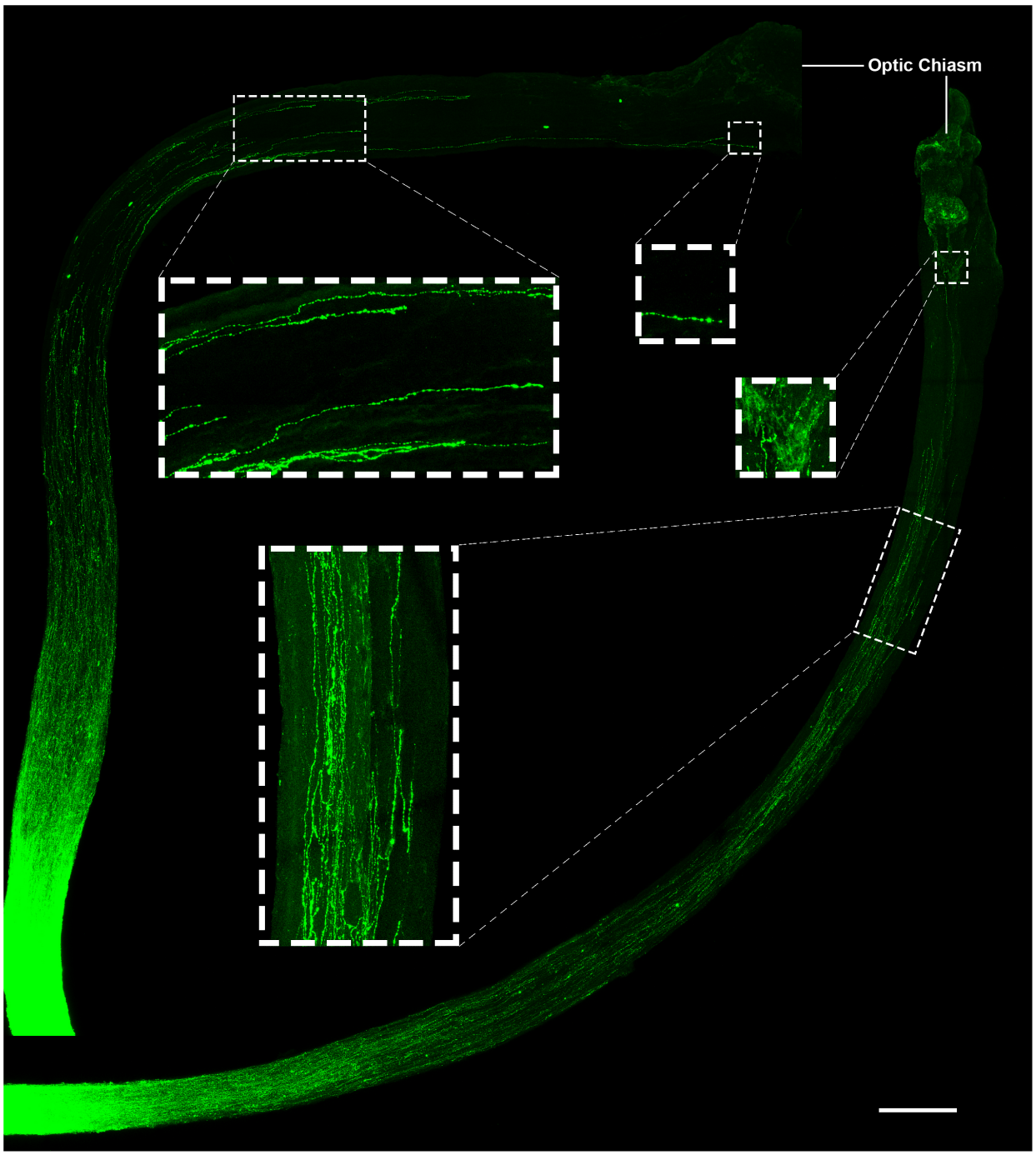

Supplementary Figure 4. Combination of myosin IIA/B deletion and Lin28a overexpression greatly enhanced optic nerve regeneration up to the optic chiasm. Related to Figure 2.

Images of two optic nerves in the combinatory treatment group with longest axons reaching optic chiasm. Magnified images show detailed morphologies of axons in white dashed boxes. Scale bar, 200 µm (66.7 µm for the magnified images).

Supplementary Figure 5

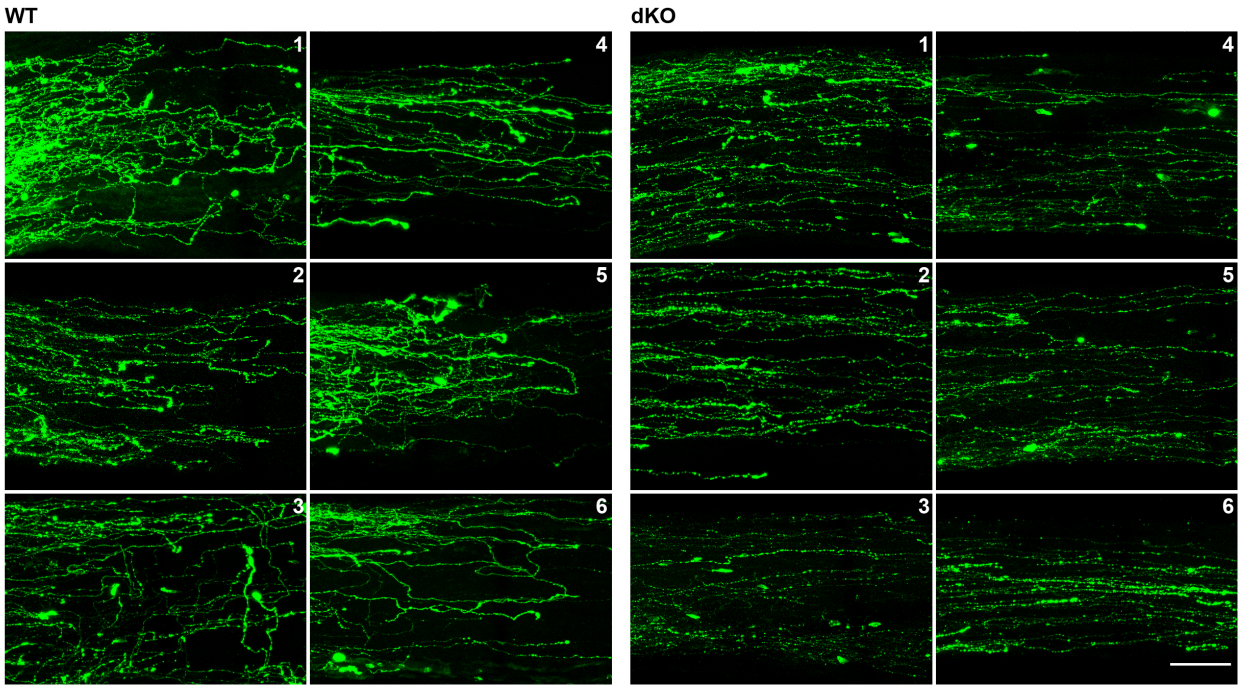

Supplementary Figure 5. Deletion of myosin IIA/B in RGCs improved axon extension efficiency. Related to Figure 5.

Images of the regions used for the quantification of axon extension efficiency (one region from each optic nerve). Scale bar, 50 μm. WT, wild type; dKO, double knockout of myosin IIA/B.

Supplementary Figure 6

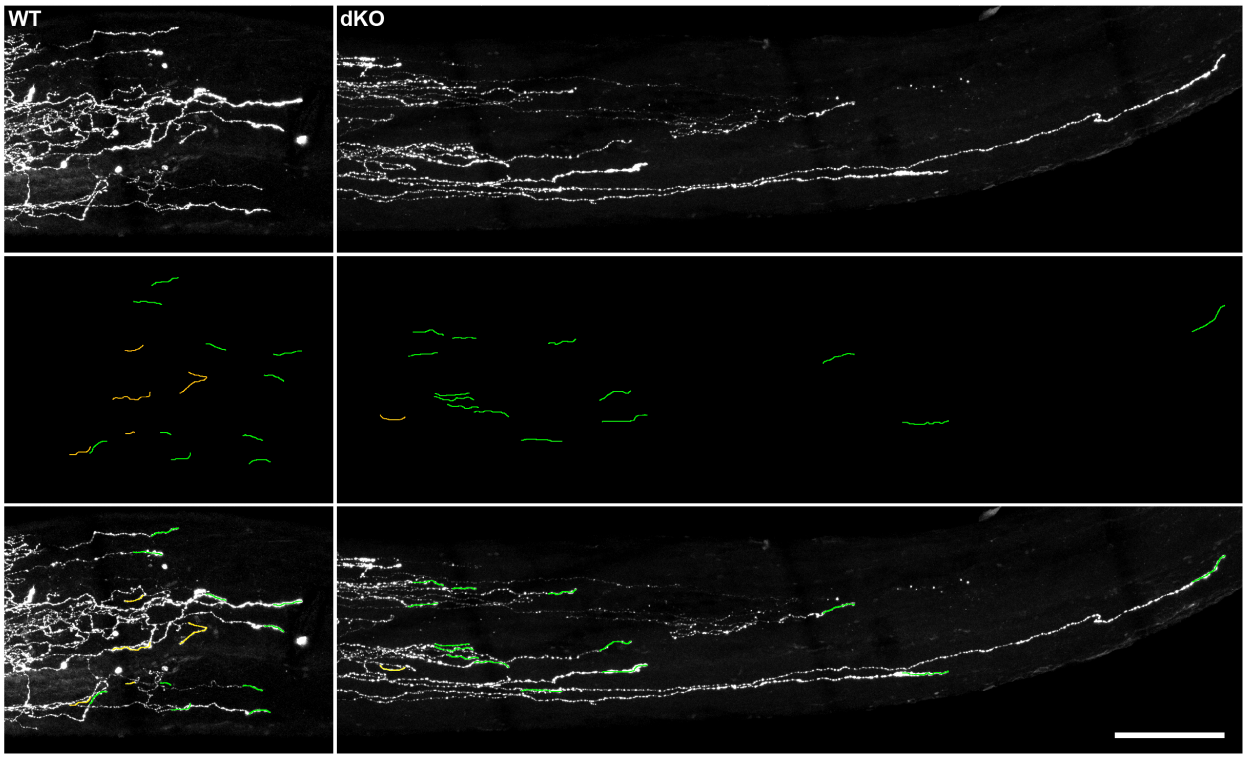

Supplementary Figure 6. Deletion of myosin IIA/B reduced U-turn rate. Related to Figure 5.

Top: representative images of the leading-edge area of optic nerves showing that myosin IIA/B deletion reduced U-turn rate. Middle: axon trajectories near axonal tips, U-turns are labeled in yellow. Bottom: overlay of top and middle rows. Scale bar, 50 μm. WT, wild type; dKO, double knockout of myosin IIA/B.